Electric field effect on electron gas spins in two-dimensional magnets with strong spin-orbit coupling

K. S. Denisov *

Ioffe Institute, 194021 St. Petersburg, Russia
and Lappeenranta-Lahti University of Technology LUT, FI-53851 Lappeenranta, Finland

(Received 10 September 2021; revised 3 December 2021; accepted 3 January 2022; published 18 January 2022)

The recent rise of material platforms combining magnetism and two-dimensionality of mobile carriers reveals a diverse spectrum of spin-orbit phenomena and stimulates its ongoing theoretical discussions. In this paper, we use the density matrix approach to provide a unified description of subtle microscopic effects governing the electron gas spin behavior in the clean limit upon electric perturbations in two-dimensional magnets with strong spin-orbit coupling. We discuss that an inhomogeneity of electrostatic potential generally leads to the electron gas spin tilting with the subsequent formation of equilibrium skyrmionlike spin textures and demonstrate that several microscopic mechanisms of two-dimensional electron gas (2DEG) spin response are equally important for this effect. We analyze the dynamics of 2DEG spin upon an oscillating electric field with a specific focus on the emergent electric dipole spin resonance. We address the resonant enhancement of magneto-optical phenomena from the spin precession equation perspective and discuss it in terms of the resonant spin generation. We also clarify the connection of both static and dynamic spin phenomena arising in response to a scalar perturbation with the electronic band Berry curvature.

DOI: 10.1103/PhysRevB.105.045413

I. INTRODUCTION

The recent advances in the development of spintronics devices extensively use relativistic spin-orbit properties of free carriers interacting with magnetic layers. The spin-orbit coupling (SOC) of charge carriers generally opens up the possibility to deal with the magnetization purely by electrical means; the magnetization orientation can be detected electrically by virtue of the anisotropic magnetoresistance effect [1–3], while electric current-induced spin-orbit torque occurs to be a highly effective tool for switching its direction [4–7]. Nonstationary dynamics of carriers in the presence of SOC can result in stimulated photon emission, as in the case of terahertz spintronic light emitters [8–11] and spin Hall nano-oscillators [12,13]. Apart from kinetic phenomena, spin-orbit effects can modify equilibrium spin configurations via indirect exchange interaction [14–16] and lead to the formation of magnetic skyrmions [17,18] due to Dzyaloshinskii-Moriya terms [19,20].

An efficient charge-to-spin conversion wanted for modern spintronics needs is often realized when turning to a two-dimensional electron gas (2DEG) [21], as the reduction of the dimensionality tends to be accompanied by the lowering of symmetry and by the subsequent increase in SOC [19,22]. There are an increasing number of different material platforms that allow one to combine systematically stronger SOC magnitudes of 2D electrons directly with a magnetic component; the examples include van der Waals heterostructures [23] either proximitized by magnetic layer [24–28] or being intrinsic ferromagnets [29–32], semiconductor nanostructures doped by magnetic dopants [33–35], surface states of magnetic topological insulators [36,37], and layered magnetic heterostructures [19,38]. Moreover, combining magnetism with 2D conductive channels additionally offers functionalities such as spin tunnel field-effect transistors [39], spin inversion effect [25], and unique classes of spinterfaces [40].

To fully benefit from two-dimensional magnetic systems, it is of key importance to have a comprehensive understanding of how the spin density of electron gas in a 2D channel responds to an applied electric field, that is, the understanding of free electron gas magnetoelectric properties. However, a complete microscopic treatment of the related phenomena appears to be extremely challenging, even despite there being a few theoretical approaches effectively dealing with multiband systems (e.g., wave-packet dynamics theory [41–45] and diagrammatic and *ab initio* calculations [46–50]). The difficulty lies in the fact that in spin-orbital systems, multiple microscopic mechanisms of quite a subtle character often contribute on the equal footing, which hinders a simplified consideration.

For instance, to restore a complete microscopic picture behind the spin accumulation and the associated spin-orbit torques in a bilayered magnetic system, one has to account for the nonequilibrium [51,52], intrinsic [50,53], and disorder-induced scenarios [54,55] of the inverse spin galvanic effect (iSGE) at the interface, as well as for the overall spin Hall current [56–58] induced in the neighbor nonmagnetic layer. Also, an exchange interaction induced spin splitting in combination with strong spin-orbit coupling generally leads to a geometrical structure of electronic band states featured by nonzero Berry curvature in k space. Treating different spin-related phenomena with account for the electronic band geometry remains an ongoing discussion. It covers, for instance, the issues of the Liouville's theorem with account for the Berry phase [59–61], the Hall conductivity modifications in presence of real-space magnetic textures [62], or, concerning the anomalous and spin Hall effects, the interplay between Karplus-Luttinger anomalous velocity and disorder-induced mechanisms [63–66]; the latter have recently been enriched

* denisokonstantin@gmail.com

by the electron scattering on a pair of impurities [66,67]. Moreover, when calculating spin-related quantities a specific class of coarse graining effects should be taken into account, as clearly demonstrated in Refs. [42,44].

In this paper, we respond to an ever-growing role that two-dimensional magnetic systems play for spintronics and consider in detail a complex pattern of microscopic effects relevant for the magnetoelectric behavior of 2DEG in the clean limit. Based on the density matrix approach, we describe the most significant spin-response mechanisms of two-dimensional spin-orbital systems within the unified framework, reveal the interconnection between different microscopic effects and clarify its relation to an electronic band geometry.

The theoretical model and the density matrix description are formulated in Sec. II. In Sec. III, we analyze a magnetoelectric effect in thermal equilibrium, namely, we consider the formation of equilibrium spin textures arising due to an inhomogeneous electrostatic potential. We discuss in detail semiclassical electron dynamics with account for a spin-to-momentum locking and identify microscopic mechanisms responsible for the magnetoelectric response. Namely, we attribute the generation of an extra-spin density directed within a 2DEG plane both to the nonadiabatic correction due to the electron spin precession and to the correlated change in charge and spin electron densities; the latter scenario is sometimes referred to as spin-dipole effect [42]. We provide a unified treatment of these mechanisms using the density matrix, derive general equations governing the contribution due to each mechanism independently, and reveal the role that the Berry curvature plays for the emergent phenomena. Numerical estimates demonstrate that the direction of equilibrium spin density of 2DEG in the presence of smooth scalar disorder can significantly alter from the host magnetization direction for a wide group of material platforms with quite different strengths of spin-orbit and exchange interactions.

In Sec. IV, we turn to the dynamical regime and investigate the 2DEG spin dynamics upon an oscillating electric field. We focus specifically on spin resonance phenomena due to electric dipole transitions, also referred to as the electric dipole spin resonance (EDSR). We derive the precession equation for 2DEG spin density capturing the spin resonance scenario, and clarify the relation of the band states' Berry curvature with the spin response susceptibility. We also discuss the spin resonance in terms of optical conductivity and describe the associated magneto-optical properties of 2DEG. In particular, we describe how the EDSR-induced generation of the in-plane spin density is accompanied by the resonant enhancement of the Hall conductivity; the latter is responsible for magneto-optical Kerr and Faraday effects. We classify different spin polarizations emerging in the dynamical regime and present analytic expressions for the spin resonance related optical conductivity.

II. THEORETICAL FRAMEWORK

A. Model band structure

We consider a 2DEG with parabolic bands affected both by the Rashba effect and by an exchange interaction with a magnetic host. We assume that the magnetization responsible for the spin splitting is directed along the z axis perpendicular to the electron motion plane. The so-called Rashba ferromagnet model covers all the physics relevant for our consideration and allows one to address the related spin phenomena in the most transparent way. The effective Hamiltonian describing this model is given by

$$\mathcal{H}(\boldsymbol{k}) = \frac{\boldsymbol{k}^2}{2m} + \boldsymbol{\Omega}_k \cdot \hat{\boldsymbol{S}}. \tag{1}$$

Here the first term describes the parabolic dispersion with an effective mass m, and $\boldsymbol{\Omega}_k$ is an effective k-space magnetic field acting on the electron spin $\hat{\boldsymbol{S}} = \hat{\boldsymbol{\sigma}}/2$; $\hat{\boldsymbol{\sigma}}$ is the vector of Pauli matrices. The field $\boldsymbol{\Omega}_k$ leads to a spin splitting of the electronic subbands; in our model $\boldsymbol{\Omega}_k$ consists of two parts,

$$\boldsymbol{\Omega}_k = \boldsymbol{\Omega}^{\mathrm{so}}(\boldsymbol{k}) - \Omega_0 \boldsymbol{e}_z, \qquad \boldsymbol{\Omega}^{\mathrm{so}}(\boldsymbol{k}) = 2\lambda_{\mathrm{so}}[\boldsymbol{e}_z \times \boldsymbol{k}], \tag{2}$$

where $\boldsymbol{\Omega}^{\mathrm{so}}(\boldsymbol{k})$ describes the spin-orbit Rashba interaction with the coupling constant λ_{so} and the second term is due to an exchange interaction with a magnetic background; the parameter Ω_0 describes the corresponding splitting of spin subbands at zero momentum. The eigenstates of the Eq. (1) Hamiltonian can be written in the following form: $\psi_k^{\pm} = e^{i\boldsymbol{k}\boldsymbol{r}}|u_k^{\pm}\rangle$, where

$$|u_k^{+}\rangle = \frac{1}{\sqrt{2}}\begin{pmatrix} b_k \\ -ie^{i\varphi}a_k \end{pmatrix}, \quad |u_k^{-}\rangle = \frac{1}{\sqrt{2}}\begin{pmatrix} -ie^{-i\varphi}a_k \\ b_k \end{pmatrix}, \tag{3}$$

and $(a_k, b_k) = (1 \pm \Omega_0/\Omega_k)^{1/2}$. We use the notation $\eta = (\pm)$ for two-electron spin subbands. The states ψ_k^{η} are characterized by the electron spin $\boldsymbol{s}_k^{\eta} = \langle u_k^{\eta}|\hat{\boldsymbol{S}}|u_k^{\eta}\rangle$ directed either parallel or antiparallel to $\boldsymbol{\Omega}_k$,

$$\boldsymbol{s}_k^{\pm} = \pm\frac{1}{2}\boldsymbol{n}_k, \quad \boldsymbol{n}_k = \frac{\boldsymbol{\Omega}_k}{\Omega_k}, \quad \Omega_k = \sqrt{\Omega_0^2 + (2\lambda_{\mathrm{so}}k)^2}, \tag{4}$$

where the unit vector $\boldsymbol{n}_k$ points along $\boldsymbol{\Omega}_k$.

The energy dispersion corresponding to η subband is $\varepsilon_k^{\eta} = k^2/2m + \eta\Omega_k/2$. The presence of k-dependent spin splitting leads to the renormalization of effective masses near $k \approx 0$, namely, $m^{\pm} = m/(1 \pm \xi)$, where the parameter $\xi \equiv 2m\lambda_{\mathrm{so}}^2/\Omega_0$. We focus on systems with sufficiently strong exchange interaction, when Ω_0 greatly exceeds the spin-orbital coupling. We thus take the parameter $\xi < 1$, at which the effective mass $m^{-} > 0$ is positive and the lower energy branch is a monotonic function of the momentum.

Let us discuss the role of the spin splitting terms. The presence of the Rashba effect induced spin-momentum locking directly manifests itself in the velocity operator

$$\hat{\boldsymbol{v}} = \frac{\partial\hat{\mathcal{H}}(\boldsymbol{k})}{\partial\boldsymbol{k}} = \frac{\boldsymbol{k}}{m} + \lambda_{\mathrm{so}}[\hat{\boldsymbol{\sigma}} \times \boldsymbol{e}_z], \tag{5}$$

where the second term is sensitive to the instantaneous direction of the electron spin. While the average velocity for the eigenspin states is determined by the unperturbed spin vector $\boldsymbol{s}_k^{\eta}$,

$$\boldsymbol{v}_k^{\eta} \equiv \langle u_k^{\eta}|\hat{\boldsymbol{v}}|u_k^{\eta}\rangle = \frac{\boldsymbol{k}}{m} + 2\lambda_{\mathrm{so}}[\boldsymbol{s}_k^{\eta} \times \boldsymbol{e}_z], \tag{6}$$

the changes in the direction of an electron spin caused by external fields can directly affect the average of the velocity operator and, correspondingly, influence the orbital motion.

The presence of a magnetic gap due to the magnetization directed perpendicular to the 2DEG plane leads additionally to the fact that electron band states acquire a geometric

structure. Indeed, the electron spin direction in $\boldsymbol{k}$ space forms a hedgehog pattern which underlies the appearance of the Berry curvature $\mathcal{F}_k^\eta = i\langle\nabla_{\boldsymbol{k}} u_k^\eta| \times |\nabla_{\boldsymbol{k}} u_k^\eta\rangle$. For a spin-1/2 Hamiltonian, the Abelian Berry curvature in $\eta = (\pm)$ subband can be expressed as follows:

$$\mathcal{F}_k^\eta = \eta \frac{1}{4\pi} \boldsymbol{n}_k \cdot \left[\frac{\partial \boldsymbol{n}_k}{\partial k_x} \times \frac{\partial \boldsymbol{n}_k}{\partial k_y}\right] = \eta\, 2\lambda_{\rm so}^2 \frac{\Omega_0}{\Omega_k^3}, \tag{7}$$

and we keep the notation $\mathcal{F}_k = |\mathcal{F}_k^\eta|$ for its absolute value. The total Berry flux Q_F^η accumulated by electrons from the η subband up to the Fermi energy μ is given by

$$Q_F^\eta = \int\limits_{k<k_F^\eta} d\boldsymbol{k}\, \mathcal{F}_k^\eta = \eta \frac{1}{4\pi}\left(1 - \frac{\Omega_0}{\Omega_F^\eta}\right), \tag{8}$$

where $\Omega_F^\eta = [\Omega_0^2 + (2\lambda_{\rm so} k_F^\eta)^2]^{1/2}$ is the spin splitting energy for $\eta = (\pm)$ subbands at the Fermi energy.

B. Density matrix approach

Let us first discuss the structure of the density matrix f^0 for 2DEG in thermal equilibrium without external perturbations. The general form is $f^0 = [e^{\beta(\hat{\mathcal{H}}-\mu)} + 1]^{-1}$, where $\hat{\mathcal{H}}$ is given by Eq. (1), β is the inverse temperature, and μ is the Fermi energy. In this paper, we focus on zero-temperature limit $\beta \to \infty$. The density matrix $\hat{f}_k^0$ in the momentum representation is a 2×2 matrix which can be presented as follows (we keep hats for spin indices only):

$$\hat{f}_k^0 = \frac{1}{2} n_k^0 + \boldsymbol{S}_k^0 \cdot \hat{\boldsymbol{\sigma}}. \tag{9}$$

We note that $\hat{f}_k^0$ is diagonal in the basis of eigenstates $\psi_k^\pm$, so we can present it as a sum of $\eta = (\pm)$ spin subband contributions $\hat{f}_k^\eta$,

$$\hat{f}_k^0 = \hat{f}_k^+ + \hat{f}_k^-, \qquad \hat{f}_k^\eta = n_k^\eta \left(\frac{1}{2} + \boldsymbol{s}_k^\eta \cdot \hat{\boldsymbol{\sigma}}\right), \tag{10}$$

where $n_k^\eta = [e^{\beta(\varepsilon_k^\eta - \mu)} + 1]^{-1}$ is the Fermi-Dirac distribution function of electrons in the spin subband with energy ε_k^η. The terms in Eq. (9) are given $n_k^0 = n_k^+ + n_k^-$ and $\boldsymbol{S}_k^0 = n_k^+ \boldsymbol{s}_k^+ + n_k^- \boldsymbol{s}_k^-$; here $\boldsymbol{s}_k^\eta$ corresponds to the eigenspin states from Eq. (4). The equilibrium spin density $\boldsymbol{S}_0$ is directed perpendicular to the 2DEG plane:

$$\boldsymbol{S}_0 = \frac{1}{2}\sum_k \mathrm{Sp}\big(\hat{f}_k^0 \cdot \hat{\boldsymbol{\sigma}}\big) = \boldsymbol{e}_z \Omega_0 \frac{\Omega_F^- - \Omega_F^+}{16\pi\lambda_{\rm so}^2}. \tag{11}$$

We note that when both spin subbands are populated ($\mu > \Omega_0/2$), the equilibrium spin density $S_0 = m\Omega_0/4\pi$ is independent of the Fermi energy; this is specific for the Hamiltonian from Eq. (1).

The application of a scalar potential $U(\boldsymbol{r}, t)$ deviates the electron distribution from Eq. (10). In this paper, we focus on spatially smooth perturbations ($k_F \cdot \nabla_k \ll 1$ and $\lambda_F \cdot \nabla_r \ll 1$) and study the electron gas response in the semiclassical limit. For this purpose, we introduce the Wigner density matrix $\hat{f}_k(\boldsymbol{r}, t)$ in the following form:

$$\hat{f}_k(\boldsymbol{r}, t) = \frac{1}{2} n_k(\boldsymbol{r}, t) + \boldsymbol{S}_k(\boldsymbol{r}, t) \cdot \hat{\boldsymbol{\sigma}}, \tag{12}$$

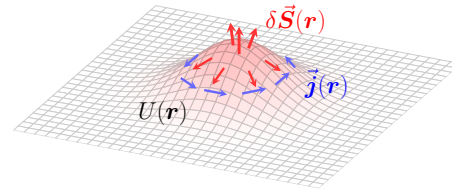

FIG. 1. Skyrmionlike distribution of the linear response spin-density perturbation and the distribution of the persistent electric currents' nearby electrostatic defects.

where $n_k(\boldsymbol{r}, t), \boldsymbol{S}_k(\boldsymbol{r}, t)$ can be treated as particle and spin distribution functions locally in real space. In particular, the 2DEG spin density perturbation emerging in the real space at point $\boldsymbol{r}$ can be found from

$$\delta\boldsymbol{S}(\boldsymbol{r}, t) = \sum_k \mathrm{Sp}(\hat{f}_k(\boldsymbol{r}, t) \cdot \hat{\boldsymbol{S}}) - \boldsymbol{S}_0 = \sum_k \boldsymbol{S}_k(\boldsymbol{r}, t) - \boldsymbol{S}_0. \tag{13}$$

The procedure to obtain the semiclassical Boltzmann equation for $\hat{f}_k(\boldsymbol{r}, t)$ is described in a number of papers [68–70] and it consists of the Wigner transformation of the von Neumann equation for the density matrix with the subsequent application of the gradient expansions. Here we omit the details and present the resulting semiclassical kinetic equation for $\hat{f}_k(\boldsymbol{r}, t)$ in the clean limit following [71]:

$$\frac{\partial \hat{f}_k}{\partial t} + \frac{1}{2}\{(\hat{\boldsymbol{v}} \cdot \nabla_{\boldsymbol{r}}); \hat{f}_k\} - [\boldsymbol{\Omega}_k \times \boldsymbol{S}_k] \cdot \hat{\boldsymbol{\sigma}} + (\boldsymbol{F} \cdot \nabla_{\boldsymbol{k}})\hat{f}_k = 0, \tag{14}$$

where $\{;\}$ stands for the anticommutator, $\nabla_{\boldsymbol{r},\boldsymbol{k}}$ are the nabla operators, $\boldsymbol{F}(\boldsymbol{r}, t) = -\nabla_{\boldsymbol{r}} U(\boldsymbol{r}, t)$ describes the dynamical force acting on electrons, and the third term takes into account the precession of the electron spin in the effective magnetic field $\boldsymbol{\Omega}_k$. It is worth noting that the semiclassical Boltzmann equation for the spin-1/2 electron can be also presented in a form directly involving SU(2) gauge fields, see the details in Ref. [69]. The latter approach has an advantage that it deals with the whole class of geometrical spin effects on equal footing, including non-Abelian phenomena in the strong spin-orbital interaction limit.

III. STATIC SPIN TEXTURES

We start our analysis by inspecting the redistribution of the 2DEG charge and spin densities' nearby smooth electrostatic defects, such as Coulomb centers or gating potential perturbations. The geometric character of electronic band states and the associated nonzero Berry curvature underline the appearance of chiral spin textures and adjoint persistent electric currents that surround electrostatic potential inhomogeneity, see Fig. 1. In Ref. [72], we used the Kubo formalism to address the nonlocal regime of the spin-density response due to short-range impurities. In this section, instead, we provide a detailed semiclassical description of this phenomenon and accompany it by comprehensive physical analysis.

A. General mechanisms of the intrinsic spin generation

Let us qualitatively discuss the effect of the electron spin nonadiabatic rotation upon the precession in a slowly varying magnetic field [50,73–75]. We start by considering the precession equation for an electron spin $\boldsymbol{s}$ rotating upon a time-dependent frequency $\boldsymbol{\Omega}(t)$:

$$\frac{d\boldsymbol{s}}{dt} = [\boldsymbol{\Omega}(t) \times \boldsymbol{s}]. \tag{15}$$

Assuming the adiabatically slow rotation of $\boldsymbol{\Omega}(t)$, i.e., that the characteristic time τ of its variation satisfies $\Omega\tau \gg 1$, the zero-order solution of the precession equation simply describes the electron spin $\boldsymbol{s}^0(t) = \boldsymbol{\Omega}(t)/2|\boldsymbol{\Omega}(t)|$ remaining coaligned with the instant direction of $\boldsymbol{\Omega}(t)$. However, the adiabatic rotation of $\boldsymbol{s}^0(t)$ can be maintained only due to the appearance of the nonadiabatic correction $\delta\boldsymbol{s}(t)$ directed perpendicular to the instant vector $\boldsymbol{\Omega}(t)$. Naturally, this correction exists in the first order in $(\Omega\tau)^{-1}$ and it can be found from the precession equation, keeping only the leading term due to $\boldsymbol{s}^0(t)$ in the time derivative:

$$\frac{d\boldsymbol{s}^0}{dt} = [\boldsymbol{\Omega}(t) \times \delta\boldsymbol{s}(t)] \quad \rightarrow \quad \delta\boldsymbol{s}(t) = \frac{1}{2\Omega^3}\left[\boldsymbol{\Omega} \times \frac{d\boldsymbol{\Omega}}{dt}\right]. \tag{16}$$

The appearance of $\delta s \propto (\Omega\tau)^{-1}s^0$ is a general property of the precession equation. Naturally, this is also valid when a Larmor frequency stems from an effective magnetic field in k space due to a spin-orbit coupling. In this case, however, the vector $\boldsymbol{\Omega}_k$ that governs the spin dynamics of an electron with momentum $\boldsymbol{k}$ varies in time only provided that the electron momentum does not remain constant along its trajectory $\dot{\boldsymbol{k}} \neq 0$, which is the case if $\boldsymbol{F} \neq 0$. The nonadiabatic spin component acquired by an electron can be estimated from Eq. (16) by replacing the time derivative by $d/dt \rightarrow \dot{\boldsymbol{k}} \cdot \boldsymbol{\nabla}_{\boldsymbol{k}}$:

$$\delta\boldsymbol{s}_k = \frac{1}{2\Omega_k^3}[\boldsymbol{\Omega}_k \times (\dot{\boldsymbol{k}} \cdot \boldsymbol{\nabla}_{\boldsymbol{k}})\boldsymbol{\Omega}_k]. \tag{17}$$

We conclude that an electron moving along its classical trajectory with finite acceleration has its spin always slightly tilted compared to the instantaneous direction of $\boldsymbol{\Omega}_k$. Moreover, in view of the spin-momentum locking, such an intrinsically generated extra spin leads to the change in the electron velocity $\delta\boldsymbol{v}_k = 2\lambda_{\rm so}(\delta\boldsymbol{s}_k \times \boldsymbol{e}_z)$.

The second spin-related phenomenon important for the collective response of 2DEG concerns the spin-dipole effect [42]. This mechanism is relevant when the single electron density $|\psi(\boldsymbol{r})|^2$ deviates from the homogeneous distribution and acquires some finite $\boldsymbol{r}$ dependence near an inhomogeneity. Let us consider an electron at the unperturbed plane-wave state $\psi_k^{\pm}$ from Eq. (3) with momentum $\boldsymbol{k}$; its spin $\boldsymbol{s}_k^{\pm}$ is determined by $\boldsymbol{\Omega}_k$. The corresponding density $|\psi_k^{\pm}|^2$ is spatially homogeneous. In fact, the smooth spatial variation of the density for such an electron is possible only provided that its wave function gets an admixture of other plane-wave band states $\psi_{k'}^{\pm}$ with momenta $\boldsymbol{k}'$ slightly differing from $\boldsymbol{k}$. Essentially, the added states have different spin orientations $\boldsymbol{s}_{k'}^{\pm} \neq \boldsymbol{s}_k^{\pm}$, so the resulting average spin density appears to be slightly tilted. In terms of the wave-packet dynamics [42,76], the mixing of spin-orbital states leads to the fact that the charge and spin centers of the electron wave packet do not coincide, which creates an additional spin polarization. This scenario is specifically important for localized electron states [77,78]. We emphasize that the spin-dipole effect is essentially connected with the spatial variation of the electron density. In particular, if a given external field keeps an electron gas in the homogeneous state, the spin-dipole contribution will be absent. The appearance of the nonadiabatic correction from Eq. (17), on the contrary, is not connected with the change of an electron density, it simply tracks the exact electron spin dynamics along quasiclassical trajectories.

We note that in systems with strong spin-orbital coupling, the electron dynamics in the clean limit exhibit a rich pattern of different effects, see Refs. [79–81]. In this paper, we focus on the microscopic phenomena described above, which are specifically important for 2D magnets.

B. Density matrix in a static inhomogeneous setting

We proceed with giving a rigorous description of the outlined phenomena based on the kinetic equation for the density matrix. Let us consider an electron gas subjected to an electrostatic potential $U(\boldsymbol{r})$ smoothly varying in space. Since the unperturbed density matrix $\hat{f}_k^0 = \hat{f}_k^+ + \hat{f}_k^-$ given by Eq. (10) has two parts corresponding to $\eta = (\pm)$ subband states, the linear response correction $\delta\hat{f}_k(\boldsymbol{r}) = \hat{f}_k(\boldsymbol{r}) - \hat{f}_k^0$ will be determined independently by two subband terms $\delta\hat{f}_k(\boldsymbol{r}) = \delta\hat{f}_k^+(\boldsymbol{r}) + \delta\hat{f}_k^-(\boldsymbol{r})$. We present the corresponding correction $\delta\hat{f}_k^{\eta}$ as follows:

$$\delta\hat{f}_k^{\eta}(\boldsymbol{r}) = \frac{1}{2}\delta n_k^{\eta}(\boldsymbol{r}) + \delta\boldsymbol{S}_k^{\eta}(\boldsymbol{r}) \cdot \hat{\boldsymbol{\sigma}}, \tag{18}$$

where $\delta n_k^{\eta}(\boldsymbol{r})$, $\delta\boldsymbol{S}_k^{\eta}(\boldsymbol{r})$ are the perturbations of the electron density and spin distribution functions, respectively.

The key suggestion implemented in this paper is to use the following ansatz for the linear response spin density:

$$\delta\boldsymbol{S}_k^{\eta}(\boldsymbol{r}) = \delta n_k^{\eta}(\boldsymbol{r})\boldsymbol{s}_k^{\eta} + n_k^{\eta}\delta\boldsymbol{s}_k^{\eta}(\boldsymbol{r}) + \delta\boldsymbol{\mathcal{S}}_k^{\eta}(\boldsymbol{r}), \tag{19}$$

where we took into account all possible types of $\delta\boldsymbol{S}_k^{\eta}(\boldsymbol{r})$ variation. Indeed, the first term describes the change of the electron spin distribution due to the change in the density δn_k^{η}. The second term corresponds to the change of the spin vector $\delta\boldsymbol{s}_k^{\eta}$ for each individual electron independently of the electron number distribution. The third term is the remaining linear-order variation, which is essentially neither due to $\delta n_k^{\eta}(\boldsymbol{r})$ nor $\delta\boldsymbol{s}_k^{\eta}(\boldsymbol{r})$ separately; thus $\delta\boldsymbol{\mathcal{S}}_k^{\eta}$ describes the correlated change of both the electron spin and charge densities. Naturally, the second and third terms in this expansion turn out to describe the nonadiabatic spin tilting and the spin-dipole effects, respectively.

We proceed with calculating $\delta\boldsymbol{S}_k^{\eta}(\boldsymbol{r})$ from the kinetic Eq. (14). Taking the trace over Eq. (14) and keeping only the terms linear in spatial gradient $\boldsymbol{\nabla}_r U$, we get

$$\left(\boldsymbol{v}_k^{\eta} \cdot \boldsymbol{\nabla}_r\right)\delta n_k^{\eta} + (\boldsymbol{F}(\boldsymbol{r}) \cdot \boldsymbol{\nabla}_k)n_k^{\eta} = 0. \tag{20}$$

Here $\boldsymbol{v}_k^{\eta}$ is the electron group velocity given by Eq. (6). The correction δn_k^{η} appears in zeroth order with respect to the spatial gradients and is given by $\delta n_k^{\eta}(\boldsymbol{r}) = U(\boldsymbol{r})(\partial n_k^{\eta}/\partial\varepsilon)$, where ε is the electron energy. The change in the overall 2DEG density is $\delta n(\boldsymbol{r}) = \delta n^+(\boldsymbol{r}) + \delta n^-(\boldsymbol{r})$, where $\delta n^{\eta}(\boldsymbol{r}) = -\nu_F^{\eta} U(\boldsymbol{r})$ and

ν_F^η is the density of states in η subbands taken at the Fermi energy. Correspondingly, the perturbation of the spin density Eq. (13) due to the first term in Eq. (19) is given by

$$\delta \boldsymbol{S}^{(1)}(\boldsymbol{r}) = \sum_{k,\eta} \boldsymbol{s}_k^\eta \delta n_k^\eta(\boldsymbol{r}) = \boldsymbol{e}_z \Omega_0 \left(\frac{\nu_F^+}{\Omega_F^+} - \frac{\nu_F^-}{\Omega_F^-} \right) U(\boldsymbol{r}). \quad (21)$$

The term $\delta \boldsymbol{S}^{(1)}(\boldsymbol{r})$ is responsible for the change in the out-of-plane spin density component and it appears even if there is no spin-orbit interaction.

A complex spin-orbital electron dynamics is responsible for an extra spin response described by $\delta \boldsymbol{s}_k^\eta$ and $\delta \boldsymbol{\mathcal{S}}_k^\eta$. We notice that these terms are absent in a homogeneous setting; thus the expansion of $\delta \boldsymbol{s}_k^\eta$, $\delta \boldsymbol{\mathcal{S}}_k^\eta$ starts with the linear term $\nabla_r U$. Taking the trace over Eq. (14) multiplied by $\hat{\boldsymbol{\sigma}}$ and keeping only terms linear in $\nabla_{\boldsymbol{r}}$, we get

$$\left[\boldsymbol{\Omega}_k \times \delta \boldsymbol{s}_k^\eta(\boldsymbol{r}) \right] - (\boldsymbol{F}(\boldsymbol{r}) \cdot \nabla_k) \boldsymbol{s}_k^\eta = 0, \quad (22)$$

$$\left[\boldsymbol{\Omega}_k \times \delta \boldsymbol{\mathcal{S}}_k^\eta(\boldsymbol{r}) \right] + \left[\boldsymbol{s}_k^\eta \times \left(\boldsymbol{s}_k^\eta \times \boldsymbol{\Omega}^{\mathrm{so}}(\nabla_r n_k^\eta) \right) \right] = 0, \quad (23)$$

where $\boldsymbol{\Omega}^{\mathrm{so}}(\nabla_r n_k^\eta)$ is obtained from Eq. (2) by replacing $\boldsymbol{k} \to \nabla_r n_k^\eta(\boldsymbol{r})$.

Let us comment on the relation between $\delta \boldsymbol{s}_k^\eta$, $\delta \boldsymbol{\mathcal{S}}_k^\eta$ and the previously described kinematic effects. The first equation, Eq. (22), can be satisfied by changing the electron spin vector $\delta \boldsymbol{s}_k^\eta$ independently of a particular density distribution n_k^η; it thus indeed describes the spin rotation of individual electrons due to the precession in the effective magnetic field $\boldsymbol{\Omega}_k$. Naturally, the nonzero term $\delta \boldsymbol{s}_k^\eta$ is exactly the nonadiabatic correction to the instant spin vector $\boldsymbol{s}_k^\eta$, which follows adiabatically the local direction of $\boldsymbol{\Omega}_k$. The solution of Eq. (22) replicates the result from Eq. (17):

$$\delta \boldsymbol{s}_k^\eta(\boldsymbol{r}) = \eta \frac{1}{2\Omega_k^3} [\boldsymbol{\Omega}_k \times (\boldsymbol{F}(\boldsymbol{r}) \cdot \nabla_{\boldsymbol{k}}) \boldsymbol{\Omega}_k]. \quad (24)$$

The second equation, Eq. (23), describes the appearance of $\delta \boldsymbol{\mathcal{S}}_k^\eta$; the general form of the solution is given by

$$\delta \boldsymbol{\mathcal{S}}_k^\eta(\boldsymbol{r}) = -\frac{1}{4\Omega_k^2} \left[\boldsymbol{\Omega}_k \times \boldsymbol{\Omega}^{\mathrm{so}}(\nabla_r n_k^\eta) \right]. \quad (25)$$

Importantly, the additional spin density $\delta \boldsymbol{\mathcal{S}}_k^\eta$ responds directly to the spatial gradient of the electron density $\nabla_r n_k^\eta(\boldsymbol{r})$ entering in $\boldsymbol{\Omega}^{\mathrm{so}}$. In fact, this allows us to refer to $\delta \boldsymbol{\mathcal{S}}_k^\eta$ as the correlational term: it is neither due to the independent change in the number of electrons nor due to the individual electron spin rotation. Instead, $\delta \boldsymbol{\mathcal{S}}_k^\eta$ describes the simultaneous change in the electron spin due to the variation in its spatial density; it is indeed relevant to the spin-dipole effect.

C. Interplay between microscopic mechanisms and the role of Berry curvature

The explicit evaluation of extra-spin density terms from Eqs. (24) and (25) for the Rashba ferromagnet model gives the following expressions:

$$\delta \boldsymbol{s}_k^\eta = \eta \frac{e \mathcal{F}_k}{2\lambda_{\mathrm{so}}} \boldsymbol{E}(\boldsymbol{r}) - \eta \frac{2e\lambda_{\mathrm{so}}^2}{\Omega_k^3} [\boldsymbol{k} \times \boldsymbol{E}(\boldsymbol{r})], \quad (26)$$

$$\delta \boldsymbol{\mathcal{S}}_k^\eta = -\mathcal{F}_k \frac{\Omega_k}{4\lambda_{\mathrm{so}}} \nabla_{\boldsymbol{r}} n_k^\eta(\boldsymbol{r}) + \eta \frac{\lambda_{\mathrm{so}}}{2\Omega_k^2} \boldsymbol{e}_z (\boldsymbol{\Omega}_k \cdot \nabla_{\boldsymbol{r}}) n_k^\eta(\boldsymbol{r}), \quad (27)$$

where $\mathcal{F}_k$ is the magnitude of the Berry curvature from Eq. (7), and the density gradient $\nabla_r n_k^\eta(\boldsymbol{r}) = -e\boldsymbol{E}(\boldsymbol{r})(\partial n_k^\eta / \partial \varepsilon)$ is due to the redistribution of electrons in the vicinity of an electrostatic inhomogeneity.

We note that various terms from Eqs. (26) and (27) give rise to quite different spin phenomena. For instance, the second terms in $\delta \boldsymbol{s}_k^\eta$, $\delta \boldsymbol{\mathcal{S}}_k^\eta$ depend on the electron momentum direction and they are particularly important for the generation of spin currents in nonmagnetic systems (they survive at $\Omega_0 \to 0$); the second term in $\delta \boldsymbol{s}_k^\eta$ is responsible for the universal spin Hall conductivity mechanism [75]. Below we focus on the local magnetoelectric effect, that is, the appearance of an equilibrium spin density in response to the local electric field. This phenomenon stems from the first terms in $\delta \boldsymbol{s}_k^\eta$, $\delta \boldsymbol{\mathcal{S}}_k^\eta$; they can directly generate an additional spin density at a given point in a space as they survive averaging over the electron momentum direction. Moreover, these terms can be explicitly expressed in terms of the Berry curvature; thus they are specific for topological systems.

The equilibrium spin density perturbations coupled with the Berry curvature of electronic states have only in-plane components; substituting Eqs. (26) and (27) to the spin density perturbation from Eq. (13), we get

$$\delta \boldsymbol{S}_\parallel(\boldsymbol{r}) = \sum_{k,\eta} n_k^\eta \delta \boldsymbol{s}_k^\eta(\boldsymbol{r}) + \delta \boldsymbol{\mathcal{S}}_k^\eta(\boldsymbol{r}) \equiv (\chi_t + \chi_d) \boldsymbol{E}(\boldsymbol{r}), \quad (28)$$

where the magnetoelectric susceptibilities $\chi_{t,d}$ correspond to the nonadiabatic spin tilting and spin-dipole effects, respectively. The evaluated expressions for χ_t, χ_d are given by

$$\chi_t = \frac{e}{2\lambda_{\mathrm{so}}} (Q_F^+ + Q_F^-), \quad (29)$$

$$\chi_d = -\frac{e}{2} \lambda_{\mathrm{so}} \Omega_0 \left(\frac{\nu_F^+}{\Omega_{F+}^2} + \frac{\nu_F^-}{\Omega_{F-}^2} \right), \quad (30)$$

where $Q_F^\pm$ is the total Berry flux from Eq. (8).

In Fig. 2, we plot the dependence of the overall spin-response coefficient $\chi \equiv \chi_t + \chi_d$ (solid lines) along with the partial contributions from χ_t and χ_d (dotted lines) on the electron gas Fermi energy μ. We note that the terms χ_t and χ_d are generally of the same order of magnitude; thus they are equally important to describe correctly the emergent spin patterns in 2DEG. Moreover, in the case when the electron gas populates both spin subbands $\mu > \Omega_0/2$, the overall response entirely disappears $\chi_t + \chi_d = 0$ (this feature was previously noted by Refs. [72,82]). In the opposite case when electrons fill only the lowest spin-subband $\mu < \Omega_0/2$, the terms χ_t, χ_d have opposite signs, which results in the sign-altering dependence of χ on the Fermi energy. We finally note that when either the spin-orbit coupling or the exchange interaction is absent, the coefficients $\chi_t = \chi_d = 0$ turn to zero and the corresponding equilibrium spin patterns disappear.

D. Discussion

Let us discuss the physical significance of the described phenomena. We first comment on the role that the intrinsic mechanisms described by Eqs. (26) and (27) play for a 2DEG behavior upon an electric field applied to a macroscopic volume. In this setting, the nonadiabatic spin precession scenario lies in the basis of the Karplus-Luttinger mechanism of

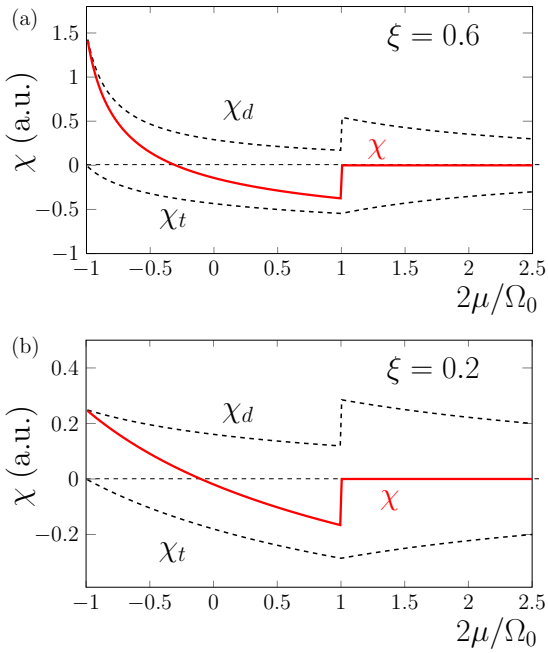

FIG. 2. The dependence of the susceptibility $\chi = \chi_t + \chi_d$ on the Fermi energy for two values of ξ parameter: (a) $\xi = 0.6$ and (b) $\xi = 0.2$

the anomalous Hall effect (AHE) [83–85], of the so-called intrinsic mechanisms of the spin Hall [75] and iSGE [6]. However, to correctly estimate the overall electron gas response on distances that greatly exceed the mean-free path, one has to additionally examine the role of disorder effects and various vertex corrections. In particular, the intrinsic contribution to AHE due to the anomalous velocity term $\delta \boldsymbol{v}_k^\eta \propto e\mathcal{F}_k^\eta \cdot [\boldsymbol{e}_z \times \boldsymbol{E}]$ tends to be canceled out by the contributions due to side-jump scattering processes [64,67,71,86]. Alternatively, the account for vertex corrections in nonmagnetic spin-orbital systems tends to eliminate the spin-orbital term from the velocity operator [87–89]. Moreover, for an accurate description of the spin accumulation phenomena, it is crucial to carefully account for the whole pattern of emergent nonequilibrium spin effects [89–93], including both the appearance of nonequilibrium spin currents near the sample boundaries [68,94,95] and dissipative iSGE mechanisms [6,21,51,58,87].

The contributions $\delta \boldsymbol{s}_k^\eta$, $\delta \boldsymbol{\mathcal{S}}_k^\eta$, however, might preserve the importance in the nondissipative regime, for instance, when the underlying electrostatic perturbation varies at distances much shorter than the mean-free path. In particular, the described equilibrium magnetoelectricity matters for 2DEG spin distribution around an ionized impurity, when the typical spatial scale under consideration is the Thomas-Fermi screening length. The distribution of an excessive 2DEG spin density emerging around an axially symmetric perturbation forms a skyrmionlike vortex pattern which is schematically shown in Fig. 1. One concludes that a smooth electrostatic potential disorder in topological spin-polarized 2DEG inevitably generates chiral spin textures, which can be particularly important for the transport properties of the corresponding system; the formation of noncollinear spin order generally leads to the topological Hall effect [96–98].

Let us give some numerical estimations for the strength of the magnetoelectric response. Since $\chi_{t,d}$ are of the same order of magnitude, we consider only the relative change in the spin density $\delta S_\parallel^t$ due to the spin-tilting mechanism. For the lower spin subband, it can be estimated as

$$\frac{\delta S_\parallel^t}{S_0} = \frac{2\lambda_{\rm so}}{\Omega_0 \Omega_F^-} eE. \tag{31}$$

One domain of material systems relevant for our analysis is semiconductor thin layers with Rashba spin-orbit interaction; the magnetism here can result from magnetic dopants (e.g., dilute semiconductors GaMnAs, CdMnTe) or be due to the proximity with a magnetic layer [24]. Keeping these systems in mind, we take common magnitudes of spin-orbit interaction $\lambda_{\rm so} = 0.65 \times 10^{-11}$ eVm [57,99–101] and the exchange spin splitting constant $\Omega_0 = 5$ meV. We let the electron gas fill only the lower spin subband and consider the concentration $n_{2D} = 7.9 \times 10^{12}$ cm^{-2} with the corresponding Fermi wave vector $k_F^- = \sqrt{4\pi n_{2D}} = 0.1$ Å^{-1} and set $\xi = 1/2$, which implies the Fermi energy $\mu = 1.4$ meV (computed according to $\mu = k_{F-}^2/2m - \Omega_F^-/2$). For this setting and typical impurity electric field $E = 10^4$ V/cm, we get a quite noticeable relative tilt of the 2DEG spin density $\delta S_\parallel^t/S_0 \sim 0.2$. Another relevant system is a polar semiconductor BiTeI tailored by vanadium dopands [35]; the latter are responsible for magnetism. We take the parameters from Ref. [35], $\lambda_{\rm so} = 3.8 \times 10^{-10}$ eVm, $\Omega_0 = 90$ meV, and put the Fermi wave vector in the lower energy branch with $k_F^- = 0.1$ Å^{-1}. We note that the lower energy branch in BiTeI is a nonmonotonic function of momentum [35] due to a larger value of $\lambda_{\rm so}$. However, for $\mu > -\Omega_0/2$, the expression for $\delta S_\parallel^t/S_0$ from Eq. (31) remains valid as it is just the total Berry flux accumulated up to the Fermi level. The similar magnitude of the effect $\delta S_\parallel^t/S_0 \sim 0.1$ is now obtained for electric fields $E = 10^5$ V/cm larger by an order of magnitude. We see that the relative change in 2DEG spin density keeps significance for quite different band parameters, so one could expect that the considered effect will also be similarly relevant for magnetic two-dimensional van der Waals materials, such as CrI_3 or $MnSe_2$ [29–32], though the real band structures in this new class of magnets can significantly alter from the Rashba ferromagnet [102,103].

The estimations given above demonstrate that an electrostatic disorder with E lying in the range $E \sim 10^4 - 10^6$ V/cm can noticeably alter the 2DEG spin density orientation from the local magnetization direction. The magnitude of this effect (up to tens of percent) is such that these perturbations should be visible via spin-polarized scanning tunneling microscopy, where the change of electron spin polarization up to several percent is experimentally accessible [104]. Alternatively, the considered magnetoelectric susceptibility of free electrons can be relevant for the magnetization control at nanoscales, namely, the generated 2DEG spin density lies in the 2D channel plane and is perpendicular to the orientation of host magnetization; thus it can contribute to torquelike effects [6]. It is worth noting a possible percolation effect emerging in a delocalized smooth electrostatic potential; namely, increasing the concentration of smooth defects each surrounded by

localized spin perturbation, one eventually reaches the percolation in terms of the appearance of a delocalized spin texture. This resembles the percolation phenomena that take place in the integer quantum Hall effect regime [105], specifically if one examines the spin-texture adjoint equilibrium currents $\boldsymbol{j}(\boldsymbol{r}) = 2e\lambda_{\rm so}[\delta\boldsymbol{S}(\boldsymbol{r}) \times \boldsymbol{e}_z]$. The presence of local equilibrium currents can maintain the orbital magnetization; this effect has been considered in Ref. [82].

The microscopic mechanisms under consideration are general for multiband systems. In Appendix A, we present the connection of our method with the wave-packet quasiclassical technique used in Refs. [41–43]. In Appendix B, we relate $\delta\boldsymbol{s}^{\eta}_{k}$, $\delta\boldsymbol{\mathcal{S}}^{\eta}_{k}$ to the Kubo formula method for the charge-spin correlation functions used in Ref. [72]. In particular, we show that the nonadiabatic spin precession is described by the interband correlation functions, while the spin-dipole effect stems from the intraband ones.

IV. SPIN DYNAMICS AND MAGNETO-OPTICAL EFFECTS

A. Electric dipole spin resonance

In this section, we focus on the electron gas spin dynamics in the presence of an oscillating electric field and describe the corresponding optical properties of a magnetic two-dimensional system. The optical response of a 2D conductive channel is generally encoded in the optical conductivity $\sigma(\omega)$. In particular, the absorption coefficient $\alpha(\omega) = (4\pi/c)\mathrm{Re}[\sigma_{xx}(\omega)]$ is connected with the longitudinal part of conductivity σ_{xx}. Also, since the time-reversal symmetry is broken in the presence of magnetism, different magneto-optical effects are possible, e.g., the magneto-optical Kerr effect (MOKE), that is, the rotation of the reflected light polarization by the complex Kerr angle ϕ_K. MOKE generally appears in a conductive media due to nonzero optical Hall conductivity $\sigma_H(\omega)$; for a 2D layer and normal incidence [106] one can express $\phi_K = \sigma_H/\sigma_{xx}\sqrt{1 + (4\pi i/\omega)\sigma_{xx}}$. Importantly, the considered geometry opens up the possibility to realize the resonant enhancement of the Hall conductivity and, thus, of the related magneto-optical effects.

Commonly, MOKE is seen to acquire a resonance structure due to interband transitions affected by the combined effect of the spin-orbit coupling and the electron spin polarization; the corresponding intrinsic contributions to the Hall conductivity at finite frequencies have been investigated in a number of papers [46,107–109]. The general idea that we are going to explore in this paper and which stands in the basis for the enhancement of magneto-optical phenomena is that the optical properties of magnetic 2D systems can be understood in terms of the EDSR. Correspondingly, the part of the optical conductivity responsible for the resonant features can be directly related to the resonantly generated spin density of 2DEG.

Let us illustrate this process in more detail; see Fig. 3. The exchange interaction field gives rise to a momentum-independent Zeeman splitting of the electron spin subbands; for the considered geometry it is directed perpendicular to the 2DEG plane. In fact, the spin-orbit interaction can be viewed as $\boldsymbol{k}$-dependent effective magnetic field $\boldsymbol{\Omega}^{\rm so}(\boldsymbol{k})$ acting on electron spins. The applied in-plane ac-electric field $\boldsymbol{E}_{\omega}e^{-i\omega t}$ causes the electron's momentum oscillations $\delta\boldsymbol{k} \propto$

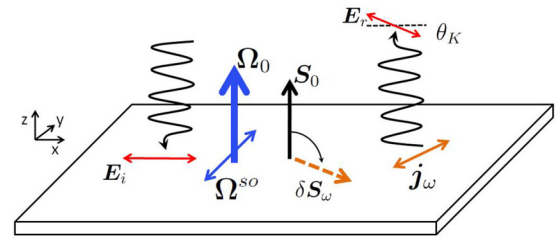

FIG. 3. The electric dipole spin resonance scheme and the appearance of MOKE due to the resonant Hall current generation $\delta\boldsymbol{j}_{\omega} = 2e\lambda_{\rm so}[\delta\boldsymbol{S}_{\omega} \times \boldsymbol{e}_z]$.

$\boldsymbol{E}_{\omega}e^{-i\omega t}$, so the associated spin-orbital field also oscillates with frequency ω. We note that $\boldsymbol{\Omega}^{\rm so}(\boldsymbol{k})$ is perpendicular to the out-of-plane exchange interaction component $\boldsymbol{\Omega}_0$. Naturally, this makes it possible to induce spin transitions when the electric field frequency coincides with the magnitude of the Zeeman spin splitting $\hbar\omega = \Omega_0$, which is exactly the EDSR scheme [110]. This spin resonance causes the equilibrium electron spin density $\boldsymbol{S}_0 \parallel \boldsymbol{e}_z$ from Eq. (11) to rotate onto the 2DEG plane, thus resonantly generating an excessive in-plane spin density $\delta\boldsymbol{S}_{\omega}$. In view of the spin-orbit coupling Eq. (5) between the velocity and spin operators, the accumulation of $\delta\boldsymbol{S}_{\omega}$ immediately leads to a resonant enhancement of the associated electric current density $\delta\boldsymbol{j}_{\omega} = 2e\lambda_{\rm so}[\delta\boldsymbol{S}_{\omega} \times \boldsymbol{e}_z]$ and of the corresponding contribution to the optical conductivity. Importantly, the in-plane spin density appears in tilted polarization with respect to the vector of the electric field, see Fig 3. In particular, the manifestation of the nonzero Berry curvature lies in the fact that there exists the perpendicular polarization of the spin density, which gives rise to the anomalous velocity $\delta\boldsymbol{v}^{\eta}_{k} \propto e\mathcal{F}^{\eta}_{k} \cdot [\boldsymbol{e}_z \times \boldsymbol{E}]$ directed perpendicular to $\boldsymbol{E}_{\omega}$ and responsible for the magneto-optical effects. The resonant generation of the spin density in this polarization leads to the enhancement of $\sigma_H(\omega)$.

B. Density matrix in the dynamical regime

Let us consider an oscillating electric field $\boldsymbol{E}_{\omega}e^{-i\omega t}$ applied in plane of the electron gas. We assume that the system remains homogeneous and present $\hat{f}_k$ in the following form:

$$\hat{f}_k(t) = \frac{1}{2}n_k(t) + \boldsymbol{S}_k(t) \cdot \hat{\boldsymbol{\sigma}}. \tag{32}$$

We keep to the high-frequency regime when ω greatly exceeds the typical inverse relaxation time $\tau_{\rm sc}^{-1}$ due to the scattering processes. The distribution function $n_k(t) = n_k + \delta n_k(\omega)e^{-i\omega t}$ satisfies the scalar part of the kinetic Eq. (14),

$$\frac{\partial n_k(t)}{\partial t} - e(\boldsymbol{E}(t) \cdot \nabla_k)n_k(t) = 0. \tag{33}$$

Since the equilibrium part contains terms from both spin subbands $n_k = n^{+}_{k} + n^{-}_{k}$, the linear response perturbation $\delta n_k(\omega) = \delta n^{+}_{k}(\omega) + \delta n^{-}_{k}(\omega)$ generally contains two contributions:

$$\delta n^{\eta}_{k}(\omega) = -\frac{e\boldsymbol{E} \cdot \boldsymbol{v}^{\eta}_{k}}{i\omega}\left(-\frac{\partial n^{\eta}_{k}}{\partial \varepsilon}\right). \tag{34}$$

The equation governing 2DEG spin dynamics is obtained

similarly to Eq. (14) and reads as

$$\frac{\partial \boldsymbol{S}_k(t)}{\partial t} - [\boldsymbol{\Omega}_k \times \boldsymbol{S}_k(t)] + e(\boldsymbol{E}(t)\cdot\nabla_k)\boldsymbol{S}_k(t) = 0. \tag{35}$$

At zero electric field, this equation describes the electron spin precession around $\boldsymbol{\Omega}_k$. The static regime solution in this case corresponds to the equilibrium spin distribution $\boldsymbol{S}_k^{\pm} \parallel \boldsymbol{\Omega}_k$ directed parallel or antiparallel to the spin splitting field, while the nonstationary solution describes the electron spin precession around $\boldsymbol{\Omega}_k$ with an eigenfrequency Ω_k. The nonzero $\boldsymbol{E}$, in turn, drives the spin dynamics due to the spin transfer in the momentum space. Naturally, when the frequency of an external field ω coincides with the precession frequency of the $\boldsymbol{k}$ electrons, the EDSR conditions are fulfilled leading to the resonant rotation. This rotation occurs with the Rabi frequency $\omega_R \propto \lambda_{\rm so}E$, which goes to zero at small electric fields. Naturally, in the case of vanishing ω_R, we can consider the linear response regime with $\boldsymbol{S}_k(t) = \boldsymbol{S}_k^0 + \delta\boldsymbol{S}_k(\omega)e^{-i\omega t}$ differing from the equilibrium value $\boldsymbol{S}_k^0 = n_k^+\boldsymbol{s}_k^+ + n_k^-\boldsymbol{s}_k^-$ by the linear-order correction $\delta\boldsymbol{S}_k(\omega)$. This is justified when the ongoing evolution of $\boldsymbol{S}_k(t)$ due to the Rabi oscillations is interrupted by the spin-relaxation processes. We thus introduce the phenomenological spin relaxation rate Γ and assume $\omega_R \ll \Gamma \ll \Omega_0$.

In the linear response regime, we can consider the spin response $\delta\boldsymbol{S}_k(\omega) = \delta\boldsymbol{S}_k^+(\omega) + \delta\boldsymbol{S}_k^-(\omega)$ independently for each spin subband (recall that $\boldsymbol{S}_k^0 = n_k^+\boldsymbol{s}_k^+ + n_k^-\boldsymbol{s}_k^-$). It is convenient to present the linearized part as

$$\delta\boldsymbol{S}_k^{\eta}(\omega) = \delta n_k^{\eta}(\omega)\boldsymbol{s}_k^{\eta} + n_k^{\eta}\delta\boldsymbol{s}_k^{\eta}(\omega), \tag{36}$$

where $\delta n_k^{\eta}(\omega)$ is determined by Eq. (34) and the equation for $\delta\boldsymbol{s}_k^{\eta}(\omega)$ is given by

$$(-i\omega+\Gamma)\delta\boldsymbol{s}_k^{\eta}(\omega) - \left[\boldsymbol{\Omega}_k \times \delta\boldsymbol{s}_k^{\eta}(\omega)\right] + e(\boldsymbol{E}_{\omega}\cdot\nabla_k)\boldsymbol{s}_k^{\eta} = 0. \tag{37}$$

Let us introduce the notation $\delta\boldsymbol{s}_{k0}^{\eta} \equiv \delta\boldsymbol{s}_k^{\eta}(\omega\to 0)$ for the additional electron spin density from Eq. (24) emerging in the static limit, we note that $(\delta\boldsymbol{s}_{k0}^{\eta}\cdot\boldsymbol{\Omega}_k) = 0$. The third term in this equation can be presented as follows: $e(\boldsymbol{E}_{\omega}\cdot\nabla_k)\boldsymbol{s}_k^{\eta} = [\boldsymbol{\Omega}_k \times \delta\boldsymbol{s}_{k0}^{\eta}]$. The spin density perturbation $\delta\boldsymbol{s}_k^{\eta}(\omega)$ lies in the plane perpendicular to $\boldsymbol{\Omega}_k$, the two independent polarizations for $\delta\boldsymbol{s}_k^{\eta}(\omega)$ are given by $\delta\boldsymbol{s}_{k0}^{\eta}$ and $[\boldsymbol{n}_k \times \delta\boldsymbol{s}_{k0}^{\eta}]$, where $\boldsymbol{n}_k = \boldsymbol{\Omega}_k/\Omega_k$ from Eq. (4). The solution of the precession equation can be written in terms of these two vectors as follows ($\Gamma \to 0$):

$$\delta\boldsymbol{s}_k^{\eta}(\omega) = -\Omega_k^2\frac{\delta\boldsymbol{s}_{k0}^{\eta} - i\omega/\Omega_k\left[\boldsymbol{n}_k \times \delta\boldsymbol{s}_{k0}^{\eta}\right]}{(\omega-\Omega_k+i\Gamma)(\omega+\Omega_k+i\Gamma)}. \tag{38}$$

The first term is directly due to the finite-frequency evolution of the nonadiabatic spin tilt mechanism. The second term exists only at finite frequencies and it arises from the electron spin retardation in the momentum space. The denominator has a pole structure which reflects the EDSR with the multiple resonances determined by $\omega = \Omega_k$.

The resulting correction to the density matrix can be presented as a sum of two terms $\delta\hat{f}_k = e^{-i\omega t}(\delta\hat{f}_k^{\rm den} + \delta\hat{f}_k^{\rm spin})$, where $\delta\hat{f}_k^{\rm den,spin}$ take the following form:

$$\delta\hat{f}_k^{\rm den} = \frac{1}{2}\delta n_k(\omega) + (\delta n_k^+(\omega)\boldsymbol{s}_k^+ + \delta n_k^-(\omega)\boldsymbol{s}_k^-)\cdot\hat{\boldsymbol{\sigma}}, \tag{39}$$

$$\delta\hat{f}_k^{\rm spin} = (n_k^+\delta\boldsymbol{s}_k^+(\omega) + n_k^-\delta\boldsymbol{s}_k^-(\omega))\cdot\hat{\boldsymbol{\sigma}}. \tag{40}$$

The optical electric conductivity $\sigma_{\alpha\beta}(\omega)$ can be obtained by calculating the electric current density via

$$\boldsymbol{j}_{\omega} = e\sum_k {\rm Sp}\left(\left(\delta\hat{f}_k^{\rm den} + \delta\hat{f}_k^{\rm spin}\right)\hat{\boldsymbol{v}}\right). \tag{41}$$

C. Resonant spin response and optical conductivity

We start the discussion of the optical conductivity. The contribution $\delta\hat{f}_k^{\rm den}$ is related specifically to the perturbation of the electron density and it gives rise to the dominant part of the longitudinal conductivity Eq. (41):

$$\boldsymbol{j}_{\omega}^{\rm Drude} = e\sum_{k,\eta}\delta n_k^{\eta}(\omega)\boldsymbol{v}_k^{\eta} = \sigma_{xx}^0(\omega)\boldsymbol{E}_{\omega},$$

$$\sigma_{xx}^0(\omega) = \frac{ie^2}{\omega}\frac{v_{F+}^2\nu_F^+ + v_{F-}^2\nu_F^-}{2}. \tag{42}$$

This is simply the Drude conductivity at finite frequency and it describes nondissipative retardation of the 2DEG density in an ac-electric field. On the contrary, the term $\delta\hat{f}_k^{\rm spin}$ is due to the spin rotation only. This contribution is responsible for the spin resonance related phenomena and below we consider its role in more detail.

The density of an electric current $\delta\boldsymbol{j}_{\omega}$ emerging due to the spin part of the density matrix $\delta\hat{f}_k^{\rm spin}$ is coupled with an induced in-plane spin density $\delta\boldsymbol{S}_{\omega}$ of 2DEG:

$$\delta\boldsymbol{j}_{\omega} = 2e\lambda_{\rm so}[\delta\boldsymbol{S}_{\omega}\times\boldsymbol{e}_z], \tag{43}$$

$$\delta\boldsymbol{S}_{\omega} = \frac{1}{2}\sum_k {\rm Sp}\left(\delta\hat{f}_k^{\rm spin}\hat{\boldsymbol{\sigma}}\right) = \sum_{k,\eta} n_k^{\eta}\,\delta\boldsymbol{s}_k^{\eta}(\omega). \tag{44}$$

Since $\delta\boldsymbol{s}_k^{\eta}(\omega)$ generally has two polarizations, see Eq. (38), the overall spin $\delta\boldsymbol{S}_{\omega}$ and, correspondingly, the associated current $\delta\boldsymbol{j}_{\omega}$ are also featured by two independent polarizations

$$\delta\boldsymbol{S}_{\omega} = \chi_l(\omega)[\boldsymbol{e}_z\times\boldsymbol{E}_{\omega}] + \chi_H(\omega)\boldsymbol{E}_{\omega}, \tag{45}$$

$$\delta\boldsymbol{j}_{\omega} = \sigma_l(\omega)\boldsymbol{E}_{\omega} + \sigma_H(\omega)[\boldsymbol{e}_z\times\boldsymbol{E}_{\omega}], \tag{46}$$

where $\sigma_{l,H}(\omega) = -2e\lambda_{\rm so}\chi_{l,H}(\omega)$. By this, we identified the contributions to the optical conductivity related to the dynamical magnetoelectric spin susceptibility.

The correction to the longitudinal conductivity $\sigma_l(\omega)$ is related to the retardation term $[\boldsymbol{n}_k \times \delta\boldsymbol{s}_{k0}^{\eta}]$ in Eq. (38). Using the formula Eq. (26) for $\delta\boldsymbol{s}_{k0}^{\eta}$ and averaging over momentum directions, we get (below we restore the Planck's constant $\hbar$)

$$\sigma_l(\omega) = ie^2\sum_k\frac{(n_k^- - n_k^+)\hbar\omega\left(\lambda_{\rm so}^2/\Omega_k\right)}{(\hbar\omega-\Omega_k+i\Gamma)(\hbar\omega+\Omega_k+i\Gamma)}\left(1+\frac{\Omega_0^2}{\Omega_k^2}\right). \tag{47}$$

The straightforward calculation of this integral gives

$$\sigma_l(\omega) = -\frac{ie^2}{16\pi\hbar}\left[\frac{2\Omega_0^2}{\hbar\omega}\left(\frac{1}{\Omega_{\rm min}} - \frac{1}{\Omega_F^-}\right) + \left(1+\frac{\Omega_0^2}{(\hbar\omega)^2}\right)\ln\left(\frac{\hbar\omega+\Omega_F^-}{\hbar\omega-\Omega_F^-}\frac{\hbar\omega-\Omega_{\rm min}}{\hbar\omega+\Omega_{\rm min}}\right)\right], \tag{48}$$

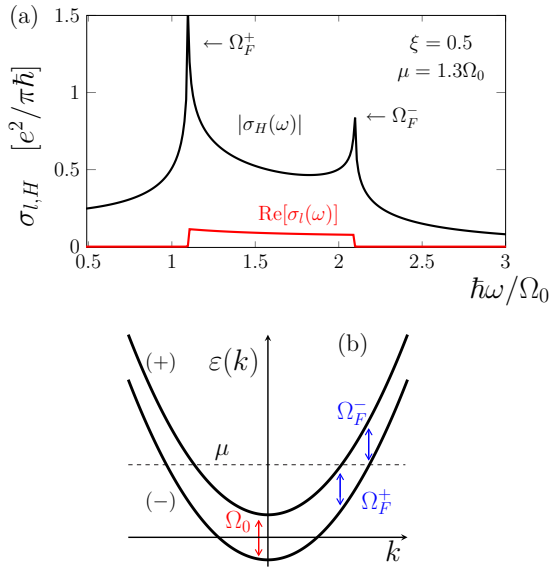

FIG. 4. (a) The dependence of optical conductivities $\sigma_{l,H}$ on frequency exhibits a resonant structure due to EDSR. (b) Electron band structure and the transition energies $\Omega_F^{\pm}$ at the Fermi level.

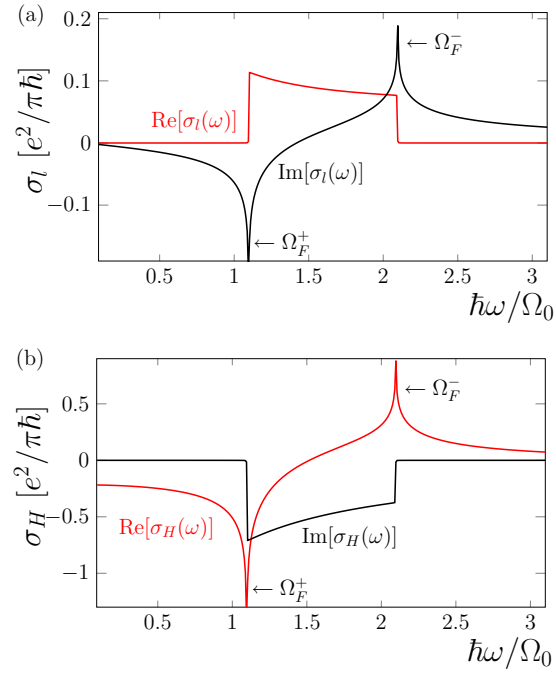

FIG. 5. The dependence of the optical conductivities $\sigma_l(\omega)$ (a) and $\sigma_H(\omega)$ (b) on the frequency ω, the parameters $\xi = 0.5$, $\mu = 1.3\,\Omega_0$.

where $\Omega_{\min} = \Omega_0$ for $\mu < \Omega_0/2$ and $\Omega_{\min} = \Omega_F^+$ for $\mu > \Omega_0/2$. The expression from above remains well-defined at $\Gamma \to 0$, though one has to keep $\hbar\omega + i\Gamma$ in the logarithm term to chose the branch of the complex function. In fact, the poles $\hbar\omega = \Omega_k$ in the denominator of $\delta s_k^{\eta}(\omega)$ lie in the continuum spectrum and the overall response of closely lying resonances merges onto the ω-regular curve featured by the Van Hove singularities at the edges of the spin splittings $\hbar\omega = (\Omega_0, \Omega_F^{\pm})$.

The real part of the longitudinal conductivity describes the energy dissipation. The presence of the resonant poles in Eq. (38) reflects the appearance of a finite absorption. Indeed, the absorption coefficient is nonzero in the frequency range $\Omega_{\min} < \hbar\omega < \Omega_F^-$ [see Fig. 4(b)] corresponding to EDSR, where its expression is given by

$$\alpha(\omega) = \frac{4\pi}{c}\mathrm{Re}[\sigma_l(\omega)] = \frac{\pi e^2}{4\hbar c}\left[1 + \left(\frac{\Omega_0}{\hbar\omega}\right)^2\right]. \tag{49}$$

We note that $\alpha(\omega)$ repeats the result for the two-dimensional massive Dirac electrons. In particular, in the limit of strong spin-orbit coupling, the magnitude of $\alpha(\omega)$ does not depend on the SOC strength and is determined by the fine structure constant.

The Hall conductivity $\sigma_H(\omega)$ stems from the Berry curvature related term in δs_{k0}^{η}. Taking into account Eqs. (26) and (38) and averaging over the momentum direction, we express $\sigma_H(\omega)$:

$$\sigma_H(\omega) = \frac{e^2}{\hbar}\sum_k \frac{(n_k^+ - n_k^-)\,\Omega_k^2\,\mathcal{F}_k}{(\hbar\omega - \Omega_k + i\Gamma)(\hbar\omega + \Omega_k + i\Gamma)}. \tag{50}$$

The evaluation of this expression gives the following result:

$$\sigma_H(\omega) = -\frac{e^2}{4\pi\hbar}\frac{\Omega_0}{\hbar\omega}\ln\left(\frac{\hbar\omega + \Omega_F^-}{\hbar\omega - \Omega_F^-}\cdot\frac{\hbar\omega - \Omega_{\min}}{\hbar\omega + \Omega_{\min}}\right). \tag{51}$$

Importantly, the Hall conductivity has the same resonance-aware logarithmic term as $\sigma_l(\omega)$.

Figure 4 demonstrates the resonant enhancement of the Hall conductivity in the EDSR absorption frequency range, namely, we plot the dependence of $\mathrm{Re}[\sigma_l(\omega)]$ and the absolute value $|\sigma_H(\omega)|$ on the electric field frequency. It is clearly seen from Fig. 4 that the increase in $|\sigma_H(\omega)|$ magnitude occurs exactly in the same frequency range where $\mathrm{Re}[\sigma_l(\omega)] \neq 0$ is nonzero. In Fig. 5, we plot the dependencies of real and imaginary parts of the spin-resonance related optical conductivities $\sigma_{l,H}(\omega)$ on frequency. The parameters are the same as in Fig. 4. The Van Hove singularities give rise to the pronounced peaks in $|\sigma_{l,H}(\omega)|$ at the boundary of the absorption band $\hbar\omega = \Omega_F^+, \Omega_F^-$. For the parameters taken in this plot ($\mu = 1.3\Omega_0$), the lower boundary is determined by Ω_F^+, see Fig. 4, as the electrons populate both spin subbands. We also note that the behavior of $\sigma_{l,H}(\omega)$ when approaching the static limit $\omega \to 0$ is different, see Fig. 5. While the longitudinal part goes to zero $\sigma_l \to 0$, the Hall conductivity has a finite nonzero limit $\sigma_H \to (e^2/\hbar)(Q_F^+ + Q_F^-)$ determined by the total Berry flux $Q_F^{\pm}$ from Eq. (8) which reflects the appearance of persistent electric currents associated with the magnetoelectric susceptibility. In the static limit, however, the accurate calculation of σ_H for a macroscopic sample requires one to take into account the disorder effect [63].

D. Discussion

The calculations of the optical conductivity of multiband systems is typically performed using the Kubo formula [46,107–109]. In Appendix C, we relate the spin polarization and the density contributions from the density matrix approach with different terms from the Kubo formalism. In Table I, we summarize the correspondence between these approaches; naturally, the spin resonance related terms are

TABLE I. Density matrix and Kubo formula correspondence.

Kubo formula	$\sigma_{xx}^{\text{intra}}$	$\sigma_{xx}^{\text{inter}}$	$\sigma_{H}^{\text{inter}}$
Density matrix	$\delta\hat{f}_k^{\text{den}}$	$n_k^\eta[\boldsymbol{n}_p \times \delta\boldsymbol{s}_{k0}^\eta]\cdot\hat{\boldsymbol{\sigma}}$	$n_k^\eta \delta\boldsymbol{s}_{k0}^\eta \cdot \hat{\boldsymbol{\sigma}}$

connected with the interband contributions σ^{inter} to the conductivity.

Let us comment on the role of spin relaxation and electron scattering. The multiple-peak structure of $\sigma_{l,H}(\omega)$ visible in Fig. 4 can be well resolved only provided that the spin-orbit interaction splitting ($|\Omega_F^{\pm} - \Omega_0| \gg \tau_{\text{sc}}^{-1}$) exceeds the energy broadening due to scattering processes. This requires rather strong spin-orbit coupling. In the opposite case, the resonance profile of $\sigma_{l,H}(\omega)$ will merge onto the single resonant-peak structure centered at Ω_0 with the line shape sensitive to particular scattering and spin relaxation processes, in analogy with EDSR of 2DEG in nonmagnetic semiconductors [111]. Interestingly, this indicates that the Hall conductivity can possess an additional information on spin relaxation times. We note that the finite absorption due to the EDSR in 2DEG is not strictly limited to the case when the Zeeman field has an out-of-plane component. In fact, most of the EDSR experiments with 2DEG in nonmagnetic semiconductors [112–114] were carried out for the in-plane magnetic field geometry. This is particularly useful when one aims to suppress the orbital quantization effects and to focus on the spin-related response only. On the contrary, combining spin-orbital electronic channels with magnetism allows one to orient the Zeeman field perpendicular to the 2DEG plane without breaking the spectrum onto Landau levels. Moreover, in this setting the electron band states are featured by the appearance of a topological structure. Experimentally studying the electronic spin resonance phenomena in these systems seems of high interest as EDSR has an extra degree of freedom that is the strong enhancement of the adjoint magneto-optical effects.

Finally, the presented interpretation of the magneto-optical effect enhancement in terms of spin resonance is equally relevant for other two-dimensional models beyond Rashba ferromagnets. For instance, e.g., massive Dirac metals [115], honeycomb lattices [116], or Haldane models [117] demonstrate similar resonant features of the Hall conductivity.

V. SUMMARY

In summary, we have considered various spin-orbital phenomena leading to a nontrivial behavior of an electron gas spin density upon application of the electric field in two-dimensional magnets. Based on the density matrix formalism, we identified different microscopic mechanisms responsible for the 2DEG spin tilting in the presence of an inhomogeneous electrostatic potential and described microscopic features of spin resonance upon an oscillating electric field with a specific focus on optical conductivity and magneto-optical phenomena. We traced the connection of the considered spin phenomena with the Berry curvature of electronic band states, thereby specifying the role of electron band topology. The presented analysis clarifies the basics of the electron gas magnetoelectric response in two-dimensional magnets and contributes to the ongoing discussion of its spintronics applications.

ACKNOWLEDGMENTS

The author thanks I. V. Rozhansky, M. M. Glazov, P. S. Alekseev, and N. S. Averkiev from the Ioffe Institute for a very fruitful discussion of the results and for giving useful advice. The work has been carried out with the financial support of the Russian Science Foundation (Project No. 18-72-10111). The author also thanks the Foundation for the Advancement of Theoretical Physics and Mathematics BASIS.

APPENDIX A: WAVE-PACKET DYNAMICS SEMICLASSICAL APPROACH

The semiclassical theory of band electrons moving in a spatially varying adiabatic perturbation $U(\boldsymbol{r})$ can be built by considering the wave-packet dynamics [44]. Let us introduce the wave packet $|W_k^n\rangle$ consisting of the nth band Bloch states $|u_k^n\rangle$, its center-of-mass coordinates in real and momentum spaces are located at $(\boldsymbol{r}_c, \boldsymbol{k})$. The average of the physical quantity Q described by operator $\hat{Q}$ can be expressed in the following way [42]:

$$Q = \sum_{k,n} f_n(\boldsymbol{k},\boldsymbol{r})\cdot\langle W_k^n|\hat{Q}|W_k^n\rangle|_{\boldsymbol{r}=\boldsymbol{r}_c} - \nabla_{\boldsymbol{r}}\cdot\sum_{k,n} f_n(\boldsymbol{k},\boldsymbol{r})\cdot\langle W_k^n|\hat{Q}\cdot(\hat{\boldsymbol{r}}-\boldsymbol{r})|W_k^n\rangle|_{\boldsymbol{r}=\boldsymbol{r}_c}, \quad \text{(A1)}$$

where the first term treats the wave packet as a point particle with the distribution function $f_n(\boldsymbol{k},\boldsymbol{r})$ and the second term is the first-order correction due to the wave-packet finite-size effects. The great advantage of this consideration is that it allows one to describe the electron dynamics in terms of semiclassical equations. For instance, in the nondissipative regime, $f_n(\boldsymbol{k},\boldsymbol{r})$ satisfies the Liouville's equation

$$\frac{df_n}{dt} = \frac{\partial f_n}{\partial t} + \{f_n;\mathcal{H}\} = 0, \quad \text{(A2)}$$

where $\mathcal{H} = \varepsilon_k^n + U(\boldsymbol{r})$ is the classical Hamiltonian function in nth electron band with energy ε_k^n. The Poisson bracket $\{A;B\}$ for A, B physical quantities depending on $(\boldsymbol{r},\boldsymbol{k})$ takes into account the kinematic Berry phase [45,60,61],

$$\{A;B\} = \omega_{\alpha\beta}\cdot(\partial_\alpha A)(\partial_\beta B), \quad \omega_{\alpha\beta} = \begin{pmatrix} \varepsilon_{\alpha\beta\gamma}\Omega_\gamma^n & \delta_{\alpha\beta} \\ -\delta_{\alpha\beta} & 0 \end{pmatrix}, \quad \text{(A3)}$$

where $(\alpha,\beta) = (\boldsymbol{r},\boldsymbol{k})$ and $\omega_{\alpha\beta}$ is the antisymmetric Poisson matrix, $\varepsilon_{\alpha\beta\gamma}$ is the Levi-Civita tensor, and $\boldsymbol{\Omega}^n$ is the Berry curvature in nth Bloch band defined as follows: $\boldsymbol{\Omega}^n = \nabla_{\boldsymbol{k}}\times\mathcal{A}_k^n = i\langle\nabla_{\boldsymbol{k}}u_k^n|\times|\nabla_{\boldsymbol{k}}u_k^n\rangle$, where $\mathcal{A}_k^n$ is the Berry connection. The expression for the Liouville's equation with account for the explicit form of $\omega_{\alpha\beta}$ is given by

$$\frac{\partial f_n}{\partial t} + \left(\frac{\partial\varepsilon_k^n}{\partial\boldsymbol{k}} + [\dot{\boldsymbol{k}}\times\boldsymbol{\Omega}_n]\right)\frac{\partial f_n}{\partial\boldsymbol{r}} + \dot{\boldsymbol{k}}\frac{\partial f_n}{\partial\boldsymbol{k}} = 0, \quad \text{(A4)}$$

where $\dot{\boldsymbol{k}} = -\nabla_{\boldsymbol{r}}\mathcal{H} = -\nabla_{\boldsymbol{r}}U(\boldsymbol{r})$. The second term in brackets describes a full electron velocity $\boldsymbol{v} = \{\mathcal{H}; \boldsymbol{r}\} = \boldsymbol{v}_k^n - [\nabla_{\boldsymbol{r}}U, \boldsymbol{\Omega}^n]$, here $\boldsymbol{v}_k^n = \nabla_k \varepsilon_k^n$.

Let us apply this technique to calculate the emerging spin density near the electrostatic inhomogeneity. We focus on the linear response regime. Following Eq. (A1), we present the spin density $\boldsymbol{S}(\boldsymbol{r})$ as follows:

$$\boldsymbol{S}(\boldsymbol{r}) = \sum_{k,n} f_n(\boldsymbol{k}, \boldsymbol{r}) \cdot \langle W_k^n | \hat{\boldsymbol{S}} | W_k^n \rangle - \nabla_{\boldsymbol{r}} \sum_{k,n} f_n(\boldsymbol{k}, \boldsymbol{r}) \langle u_k^n | \hat{\boldsymbol{S}} \big(i\nabla_{\boldsymbol{k}} - \mathcal{A}_k^n\big) | u_k^n \rangle. \tag{A5}$$

In the second term, we took into account that the wave packet $|W_k^n\rangle$ is strongly localized near $\boldsymbol{k}$ in the momentum space and we can approximate it as follows: $|W_k^n\rangle \approx e^{i\boldsymbol{k}\boldsymbol{r}}|u_k^n\rangle$, which leads us directly to the expression in Eq. (A5). The unperturbed spin density $\boldsymbol{S}_0$ corresponds to $U(\boldsymbol{r}) = 0$, at which $f_n(\boldsymbol{k}, \boldsymbol{r}) = f_n^0(\boldsymbol{k})$ and $\boldsymbol{S}_0$ is given by

$$\boldsymbol{S}_0 = \sum_{k,n} f_n^0(\boldsymbol{k}) \langle u_k^n | \hat{\boldsymbol{S}} | u_k^n \rangle. \tag{A6}$$

The linear order deviations from $\boldsymbol{S}_0$ arise from three different origins. First, the distribution function $f_n(\boldsymbol{k}, \boldsymbol{r}) = f_n^0(\boldsymbol{k}) + \delta f_n(\boldsymbol{k}, \boldsymbol{r})$ in the presence of U is modified as $\delta f_n(\boldsymbol{k}, \boldsymbol{r}) = U \partial f_n^0 / \partial \varepsilon$ according to Eq. (A4):

$$(\boldsymbol{v}_k^n \cdot \nabla_{\boldsymbol{r}}) \delta f_n(\boldsymbol{k}, \boldsymbol{r}) + \boldsymbol{F}(\boldsymbol{r}) \cdot \frac{\partial f_n^0}{\partial \boldsymbol{k}} = 0. \tag{A7}$$

Taking into account the redistribution of the electron density in the first term in Eq. (A5) and approximating $\langle W_k^n | \hat{\boldsymbol{S}} | W_k^n \rangle \approx \langle u_k^n | \hat{\boldsymbol{S}} | u_k^n \rangle$, we obtain the contribution identical with Eq. (21) in the density matrix approach:

$$\delta \boldsymbol{S}^{(1)}(\boldsymbol{r}) = \sum_{k,n} \delta f_n(\boldsymbol{k}, \boldsymbol{r}) \langle u_k^n | \hat{\boldsymbol{S}} | u_k^n \rangle. \tag{A8}$$

Also, the inhomogeneous structure of f_n gives rise to the spin-dipole contribution, that is, the second term in Eq. (A5):

$$\delta \boldsymbol{\mathcal{S}}(\boldsymbol{r}) = -\boldsymbol{F}(\boldsymbol{r}) \sum_{k,n} \left(-\frac{\partial f_n^0}{\partial \varepsilon} \right) \langle u_k^n | \hat{\boldsymbol{S}} \big(i\nabla_{\boldsymbol{k}} - \mathcal{A}_k^n\big) | u_k^n \rangle. \tag{A9}$$

The straightforward evaluation of this expression for the Rashba ferromagnet model leads to the susceptibility χ_d given by Eq. (29). Finally, there is also the linear order perturbation which is not associated with the change in the electron distribution. In fact, the first term in Eq. (A5) is determined by the average spin of an electron wave packet $\boldsymbol{s}_k^n(t) = \langle W_k^n | \hat{\boldsymbol{S}} | W_k^n \rangle$, which satisfies the precession equation:

$$\frac{d\boldsymbol{s}_k^n}{dt} = \big[\boldsymbol{\Omega}_k \times \boldsymbol{s}_k^n\big]. \tag{A10}$$

According to our discussion from Sec. III A, the wave-packet spin acquires a nonadiabatic correction $\delta \boldsymbol{s}_k^n$ linear in $\boldsymbol{F}$ and given by Eq. (17). This term gives rise to the spin perturbation $\delta \boldsymbol{S} = \sum_{(k,n)} f_n^0 \delta \boldsymbol{s}_k^n$ identical to χ_t contribution to the spin susceptibility from Eq. (29).

APPENDIX B: KUBO FORMULA IN THE STATIC LIMIT

In this Appendix, we relate the semiclassical description of magnetoelectric susceptibility in terms of the density matrix with the Kubo formula for the charge-spin correlation functions, considered in detail in Ref. [72]. The spin density induced in 2DEG by the change in the potential energy $U(\boldsymbol{r})$ is given in linear response by

$$\delta \boldsymbol{S}(\boldsymbol{r}) = \int \frac{d\boldsymbol{q}}{(2\pi)^2} e^{i\boldsymbol{q}\boldsymbol{r}} \boldsymbol{\mathcal{Q}}(\boldsymbol{q}) U(\boldsymbol{q}), \tag{B1}$$

where $U(\boldsymbol{q})$ is the Fourier component of $U(\boldsymbol{r})$ and the static charge-spin correlation function $\boldsymbol{\mathcal{Q}}(\boldsymbol{q})$ can be computed from the Kubo formula $\boldsymbol{\mathcal{Q}}(\boldsymbol{q}) = \sum_{m,n} \boldsymbol{\mathcal{Q}}^{mn}(\boldsymbol{q})$,

$$\boldsymbol{\mathcal{Q}}^{mn}(\boldsymbol{q}) = \sum_k f_k^m \frac{\langle u_k^m | \hat{\boldsymbol{S}} | u_{k+q}^n \rangle \langle u_{k+q}^n | u_k^m \rangle}{\varepsilon_k^m - \varepsilon_{k+q}^n + i0} - f_{k+q}^m \frac{\langle u_k^n | \hat{\boldsymbol{S}} | u_{k+q}^m \rangle \langle u_{k+q}^m | u_k^n \rangle}{\varepsilon_k^n - \varepsilon_{k+q}^m + i0}. \tag{B2}$$

The terms $\boldsymbol{\mathcal{Q}}^{nn}$ with $m = n$ describe the intraband contributions, while $\boldsymbol{\mathcal{Q}}^{mn}$ with $m \neq n$ correspond to the interband ones.

The Kubo formula Eq. (B2) has been explicitly evaluated for an arbitrary wave vector $\boldsymbol{q}$ in Ref. [72] for Rashba ferromagnets and Dirac models. Here we focus on the semiclassical regime when the potential U changes smoothly on the Fermi wavelength λ_F scale, so the following relation is fulfilled: $\lambda_F \cdot \nabla_r U \ll U$. In this case, the spin response becomes local and the correlation function for the Rashba ferromagnet model takes the following form: $\boldsymbol{\mathcal{Q}} = i\boldsymbol{q} \cdot \chi$, where χ is the q-independent coefficient describing the susceptibility $\delta \boldsymbol{S}(\boldsymbol{r}) = \chi \boldsymbol{E}(\boldsymbol{r})$.

We now proceed with considering the role of intra- and interband terms. In the intraband contribution $\boldsymbol{\mathcal{Q}}^{nn}$, we replace $(f_k^n - f_{k+q}^n)/(\varepsilon_k^n - \varepsilon_{k+q}^n + i0) \approx \partial f_k^n / \partial \varepsilon$ and keep only the q-linear terms in the matrix elements. With that, the expression takes the following form:

$$\boldsymbol{\mathcal{Q}}^{nn} = -i\boldsymbol{q} \sum_k \left(-\frac{\partial f_n^0}{\partial \varepsilon} \right) \langle u_k^n | \hat{\boldsymbol{S}} \big(i\nabla_{\boldsymbol{k}} - \mathcal{A}_k^n\big) | u_k^n \rangle, \tag{B3}$$

where $\mathcal{A}_k^n = i\langle u_k^n | \nabla_k u_k^n \rangle$ is the Berry connection. When taking the Fourier transform Eq. (B1), $\boldsymbol{\mathcal{Q}}^{nn}$ gives exactly the spin perturbation $\delta \boldsymbol{\mathcal{S}}$ in the form of Eq. (A9) corresponding to the spin-dipole term within the semiclassical wave-packet approach. We thus conclude that the spin-dipole effect from Eq. (29) is related to the intraband terms in the Kubo formula.

In the interband contributions $\boldsymbol{\mathcal{Q}}^{mn}$, we also keep only the linear terms with respect to $\boldsymbol{q}$, which brings us to the following expression:

$$\boldsymbol{\mathcal{Q}}^{mn}(\boldsymbol{q}) = i\boldsymbol{q} \sum_k f_k^m \, \mathrm{Re}\left(\frac{\langle u_k^n | \hat{\boldsymbol{\sigma}} | u_k^m \rangle \mathcal{A}_k^{mn}}{\varepsilon_k^m - \varepsilon_k^n} \right), \tag{B4}$$

where $\mathcal{A}_k^{mn} = i\langle u_k^m | \nabla_k u_k^n \rangle$. The straightforward calculations for the Rashba ferromagnet model with $n, m = (\pm)$ gives

$$\boldsymbol{\mathcal{Q}}^{\pm\mp}(\boldsymbol{q}) = \pm i\boldsymbol{q} \sum_k f_k^{\pm} \cdot \frac{\mathcal{F}_k}{2\lambda_{\mathrm{so}}}, \tag{B5}$$

where $\mathcal{F}_k$ is the Berry curvature from Eq. (7). The interband terms are related exactly to the nonadiabatic spin tilt effect described by $\delta \boldsymbol{s}_k^{\eta}$ in the density matrix formalism and given by χ_t susceptibility from Eq. (29).

APPENDIX C: KUBO FORMULA IN THE DYNAMICAL REGIME

In this Appendix, we relate the Kubo formula calculations of the optical conductivity with the spin resonance related terms emerging in the density matrix approach. The Kubo formula for the conductivity is given by [117,118]

$$\sigma_{\alpha\beta}(\omega) = -\frac{ie^2\hbar}{S}\sum_{k,m,n}\frac{f_k^m - f_{k+q}^n}{\varepsilon_k^m - \varepsilon_{k+q}^n}\frac{v^{\alpha}_{(k,m),(k+q,n)}v^{\beta}_{(k+q,n),(k,m)}}{\varepsilon_k^m - \varepsilon_{k+q}^n + \hbar\omega + i0}, \tag{C1}$$

where $\boldsymbol{q} \to 0$ and $\hat{\boldsymbol{v}} = \partial\hat{H}(\boldsymbol{k})/\partial\boldsymbol{k}$ is the proper matrix element of the velocity operator between i, j states. We first consider the longitudinal conductivity $\sigma_{xx}(\omega)$. The contribution to $\sigma_{xx}(\omega)$ due to intraband terms has the form

$$\sigma_{xx}^{\text{intra}}(\omega) = \frac{ie^2}{\hbar\omega}\sum_m \int d\varepsilon\, \nu_m(\varepsilon)\left(-\frac{\partial f_k^m}{\partial\varepsilon}\right)\left\langle\left|v^x_{k,m}\right|^2\right\rangle, \tag{C2}$$

where ν_m is the density of states in the corresponding band m and $\langle|v^x_{k,m}|^2\rangle$ is the angular averaged square of the matrix element modulus. This part describes the Drude conductivity at $\omega\tau_{sc} \gg 1$ due to the perturbation of the electron density and it corresponds to Eq. (42) from the main text. For the Rashba ferromagnet model, the evaluation of the integral gives

$$\sigma_{xx}^{\text{intra}}(\omega) = i\frac{e^2}{\omega}\frac{v_{F+}^2\nu_F^+ + v_{F-}^2\nu_F^-}{2}. \tag{C3}$$

The contribution to $\sigma_{xx}(\omega)$ due to interband terms in the case of the Rashba ferromagnet model has the following form:

$$\sigma_{xx}^{\text{inter}}(\omega) = \frac{ie^2}{S}\sum_k \frac{f_k^- - f_k^+}{-\Omega_k}\frac{\left\langle\left|v^x_{(k,-),(k,+)}\right|^2\right\rangle}{\hbar\omega - \Omega_k + i0} + \frac{f_k^+ - f_k^-}{\Omega_k}\frac{\left\langle\left|v^x_{(k,-),(k,+)}\right|^2\right\rangle}{\hbar\omega + \Omega_k + i0}. \tag{C4}$$

The angular averaged velocity element is $\langle|v^x_{(k,-),(k,+)}|^2\rangle = (\lambda_{\text{so}}^2/2)(1 + \Omega_0^2/\Omega_k^2)$. Using this formula and combining the denominators in $\sigma_{xx}^{\text{inter}}$ we get the following expression:

$$\sigma_{xx}^{\text{inter}} = ie^2\cdot\sum_k \frac{(f_k^+ - f_k^-)\hbar\omega\left(\lambda_{\text{so}}^2/\Omega_k\right)}{(\hbar\omega - \Omega_k + i0)(\hbar\omega + \Omega_k + i0)}\left(1 + \frac{\Omega_0^2}{\Omega_k^2}\right), \tag{C5}$$

which repeats Eq. (47) for $\sigma_l(\omega)$. We thus conclude that $\sigma_{xx}^{\text{inter}}(\omega)$ is related to $[\boldsymbol{n}_k \times \delta\boldsymbol{s}_{k0}^{\eta}]$ polarization in terms of the in-plane spin density (see Eqs. (38) and (26) from the main text).

It is instructive to analyze the energy absorption due to the spin resonance. For this purpose, we explicitly write the expression for the real part of the longitudinal conductivity due to the interband terms:

$$\text{Re}\left[\sigma_{xx}^{\text{inter}}\right] = \frac{\pi e^2}{\hbar\omega S}\sum_k (f_k^- - f_k^+)\left|v^x_{(k,-),(k,+)}\right|^2 \delta(\varepsilon_k^- - \varepsilon_k^+ + \hbar\omega). \tag{C6}$$

The expression has the form of Fermi's golden rule; its straightforward calculation leads to Eq. (49).

We now turn to the transversal component of the conductivity. The interband contribution is given by

$$\sigma_{yx}^{\text{inter}}(\omega) = \frac{ie^2}{S}\sum_k \frac{f_k^+ - f_k^-}{\Omega_k} \times\left(\frac{v^y_{(k,-),(k,+)}v^x_{(k,+),(k,-)}}{\hbar\omega - \Omega_k + i0} + \frac{\left(v^y_{(k,-),(k,+)}v^x_{(k,+),(k,-)}\right)^*}{\hbar\omega + \Omega_k + i0}\right). \tag{C7}$$

The angular averaged combination of matrix elements $\langle v^y_{-+}v^x_{+-}\rangle = -i\lambda_{\text{so}}\Omega_0/\Omega_k$ is purely imaginary. Combining both terms, we obtain

$$\sigma_{yx}^{\text{inter}}(\omega) = -\frac{e^2}{\hbar S}\sum_k \frac{(f_k^- - f_k^+)\Omega_k^2\,\mathcal{F}_k}{(\hbar\omega - \Omega_k + i0)(\hbar\omega + \Omega_k + i0)}, \tag{C8}$$

which is same the expression Eq. (50) that we get via the density matrix formalism considering $\boldsymbol{s}_{k0}$ contribution to the spin density [see Eqs. (38) and (26) from the main text].

[1] C. Gould, C. Rüster, T. Jungwirth, E. Girgis, G. M. Schott, R. Giraud, K. Brunner, G. Schmidt, and L. W. Molenkamp, Tunneling Anisotropic Magnetoresistance: A Spin-Valve-Like Tunnel Magnetoresistance using a Single Magnetic Layer, Phys. Rev. Lett. **93**, 117203 (2004).

[2] J. Moser, A. Matos-Abiague, D. Schuh, W. Wegscheider, J. Fabian, and D. Weiss, Tunneling Anisotropic Magnetoresistance and Spin-Orbit Coupling in Fe/GaAs/Au Tunnel Junctions, Phys. Rev. Lett. **99**, 056601 (2007).

[3] A. Kandala, A. Richardella, S. Kempinger, C. Liu, and N. Samarth, Giant anisotropic magnetoresistance in a quantum anomalous Hall insulator, Nat. Commun. **6**, 7434 (2015).

[4] I. Miron, G. Gaudin, S. Auffret, B. Rodmacq, A. Schuhl, S. Pizzini, J. Vogel, and P. Gambardella, Current-driven spin torque induced by the Rashba effect in a ferromagnetic metal layer, Nat. Mater. **9**, 230 (2010).

[5] I. Miron, K. Garello, G. Gaudin, P. Zermatten, M. V. Costache, S. Auffret, S. Bandiera, B. Rodmacq, A. Schuhl, and P. Gambardella, Perpendicular switching of a single ferromagnetic layer induced by in-plane current injection, Nature (London) **476**, 189 (2011).

[6] A. Manchon, J. Železný, I. M. Miron, T. Jungwirth, J. Sinova, A. Thiaville, K. Garello, and P. Gambardella, Current-induced spin-orbit torques in ferromagnetic and antiferromagnetic systems, Rev. Mod. Phys. **91**, 035004 (2019).

[7] C. Song, R. Zhang, L. Liao, Y. Zhou, X. Zhou, R. Chen, Y. You, X. Chen, and F. Pan, Spin-orbit torques: Materials, mechanisms, performances, and potential applications, Prog. Mater. Sci. **118**, 100761 (2020).

[8] T. Kampfrath, M. Battiato, P. Maldonado, G. Eilers, J. Nötzold, S. Mährlein, V. Zbarsky, F. Freimuth, Y. Mokrousov, S. Blügel *et al.*, Terahertz spin current pulses controlled by magnetic heterostructures, Nat. Nanotechnol. **8**, 256 (2013).

[9] J. Walowski and M. Münzenberg, Perspective: Ultrafast magnetism and THz spintronics, J. Appl. Phys. **120**, 140901 (2016).

[10] T. Seifert, S. Jaiswal, U. Martens, J. Hannegan, L. Braun, P. Maldonado, F. Freimuth, A. Kronenberg, J. Henrizi, I. Radu *et al.*, Efficient metallic spintronic emitters of ultrabroadband terahertz radiation, Nat. Photonics **10**, 483 (2016).

[11] Z. Feng, H. Qiu, D. Wang, C. Zhang, S. Sun, B. Jin, and W. Tan, Spintronic terahertz emitter, J. Appl. Phys. **129**, 010901 (2021).

[12] R. H. Liu, W. L. Lim, and S. Urazhdin, Spectral Characteristics of the Microwave Emission by the Spin Hall Nano-Oscillator, Phys. Rev. Lett. **110**, 147601 (2013).

[13] A. Awad, P. Dürrenfeld, A. Houshang, M. Dvornik, E. Iacocca, R. Dumas, and J. Åkerman, Long-range mutual synchronization of spin Hall nano-oscillators, Nat. Phys. **13**, 292 (2017).

[14] A. Kundu and S. Zhang, Dzyaloshinskii-Moriya interaction mediated by spin-polarized band with Rashba spin-orbit coupling, Phys. Rev. B **92**, 094434 (2015).

[15] J.-J. Zhu, D.-X. Yao, S. C. Zhang, and K. Chang, Electrically Controllable Surface Magnetism on the Surface of Topological Insulators, Phys. Rev. Lett. **106**, 097201 (2011).

[16] J. Checkelsky, J. Ye, Y. Onose, Y. Iwasa, and Y. Tokura, Dirac-fermion-mediated ferromagnetism in a topological insulator, Nat. Phys. **8**, 729 (2012).

[17] R. Wiesendanger, Nanoscale magnetic skyrmions in metallic films and multilayers: A new twist for spintronics, Nat. Rev. Mater. **1**, 16044 (2016).

[18] A. Fert, N. Reyren, and V. Cros, Magnetic skyrmions: Advances in physics and potential applications, Nat. Rev. Mater. **2**, 17031 (2017).

[19] A. Soumyanarayanan, N. Reyren, A. Fert, and C. Panagopoulos, Emergent phenomena induced by spin–orbit coupling at surfaces and interfaces, Nature (London) **539**, 509 (2016).

[20] C. Moreau-Luchaire, C. Moutafis, N. Reyren, J. Sampaio, C. Vaz, N. Van Horne, K. Bouzehouane, K. Garcia, C. Deranlot, P. Warnicke *et al.*, Additive interfacial chiral interaction in multilayers for stabilization of small individual skyrmions at room temperature, Nat. Nanotechnol. **11**, 444 (2016).

[21] M. Offidani, M. Milletarì, R. Raimondi, and A. Ferreira, Optimal Charge-To-Spin Conversion in Graphene on Transition-Metal Dichalcogenides, Phys. Rev. Lett. **119**, 196801 (2017).

[22] T. Guillet, A. Marty, C. Vergnaud, M. Jamet, C. Zucchetti, G. Isella, Q. Barbedienne, H. Jaffrès, N. Reyren, J.-M. George, and A. Fert, Large Rashba unidirectional magnetoresistance in the Fe/Ge(111) interface states, Phys. Rev. B **103**, 064411 (2021).

[23] A. Avsar, H. Ochoa, F. Guinea, B. Özyilmaz, B. J. van Wees, and I. J. Vera-Marun, *Colloquium*: Spintronics in graphene and other two-dimensional materials, Rev. Mod. Phys. **92**, 021003 (2020).

[24] I. Žutić, A. Matos-Abiague, B. Scharf, H. Dery, and K. Belashchenko, Proximitized materials, Mater. Today **22**, 85 (2019).

[25] J. Xu, S. Singh, J. Katoch, G. Wu, T. Zhu, I. Žutić, and R. K. Kawakami, Spin inversion in graphene spin valves by gate-tunable magnetic proximity effect at one-dimensional contacts, Nat. Commun. **9**, 1 (2018).

[26] P. Wei, S. Lee, F. Lemaitre, L. Pinel, D. Cutaia, W. Cha, F. Katmis, Y. Zhu, D. Heiman, J. Hone *et al.*, Strong interfacial exchange field in the graphene/EuS heterostructure, Nat. Mater. **15**, 711 (2016).

[27] H. X. Yang, A. Hallal, D. Terrade, X. Waintal, S. Roche, and M. Chshiev, Proximity Effects Induced in Graphene by Magnetic Insulators: First-Principles Calculations on Spin Filtering and Exchange-Splitting Gaps, Phys. Rev. Lett. **110**, 046603 (2013).

[28] C. Zhao, T. Norden, P. Zhang, P. Zhao, Y. Cheng, F. Sun, J. P. Parry, P. Taheri, J. Wang, Y. Yang *et al.*, Enhanced valley splitting in monolayer WSe2 due to magnetic exchange field, Nat. Nanotechnol. **12**, 757 (2017).

[29] D. Zhong, K. L. Seyler, X. Linpeng, R. Cheng, N. Sivadas, B. Huang, E. Schmidgall, T. Taniguchi, K. Watanabe, M. A. McGuire *et al.*, Van der Waals engineering of ferromagnetic semiconductor heterostructures for spin and valleytronics, Sci. Adv. **3**, e1603113 (2017).

[30] C. Gong, L. Li, Z. Li, H. Ji, A. Stern, Y. Xia, T. Cao, W. Bao, C. Wang, Y. Wang *et al.*, Discovery of intrinsic ferromagnetism in two-dimensional van der Waals crystals, Nature (London) **546**, 265 (2017).

[31] B. Huang, G. Clark, E. Navarro-Moratalla, D. R. Klein, R. Cheng, K. L. Seyler, D. Zhong, E. Schmidgall, M. A. McGuire, D. H. Cobden *et al.*, Layer-dependent ferromagnetism in a van der Waals crystal down to the monolayer limit, Nature (London) **546**, 270 (2017).

[32] D. J. OHara, T. Zhu, A. H. Trout, A. S. Ahmed, Y. K. Luo, C. H. Lee, M. R. Brenner, S. Rajan, J. A. Gupta, D. W. McComb *et al.*, Room temperature intrinsic ferromagnetism in epitaxial manganese selenide films in the monolayer limit, Nano Lett. **18**, 3125 (2018).

[33] B. Lee, T. Jungwirth, and A. H. MacDonald, Theory of ferromagnetism in diluted magnetic semiconductor quantum wells, Phys. Rev. B **61**, 15606 (2000).

[34] C. Camilleri, F. Teppe, D. Scalbert, Y. G. Semenov, M. Nawrocki, M. Dyakonov, J. Cibert, S. Tatarenko, and T. Wojtowicz, Electron and hole spin relaxation in modulation-doped CdMnTe quantum wells, Phys. Rev. B **64**, 085331 (2001).

[35] I. I. Klimovskikh, A. M. Shikin, M. Otrokov, A. Ernst, I. P. Rusinov, O. Tereshchenko, V. Golyashov, J. Sánchez-Barriga, A. Y. Varykhalov, O. Rader *et al.*, Giant magnetic band gap in the Rashba-split surface state of vanadium-doped BiTeI: A combined photoemission and ab initio study, Sci. Rep. **7**, 3353 (2017).

[36] Y. Gong, J. Guo, J. Li, K. Zhu, M. Liao, X. Liu, Q. Zhang, L. Gu, L. Tang, X. Feng *et al.*, Experimental realization of an intrinsic magnetic topological insulator, Chin. Phys. Lett. **36**, 076801 (2019).

[37] Q. L. He, X. Kou, A. J. Grutter, G. Yin, L. Pan, X. Che, Y. Liu, T. Nie, B. Zhang, S. M. Disseler *et al.*,

Tailoring exchange couplings in magnetic topological-insulator/antiferromagnet heterostructures, Nat. Mater. **16**, 94 (2017).

[38] J.-C. Rojas-Sánchez, P. Laczkowski, J. Sampaio, S. Collin, K. Bouzehouane, N. Reyren, H. Jaffrès, A. Mougin, and J.-M. George, Perpendicular magnetization reversal in Pt/[Co/Ni] 3/Al multilayers via the spin Hall effect of Pt, Appl. Phys. Lett. **108**, 082406 (2016).

[39] S. Jiang, L. Li, Z. Wang, J. Shan, and K. F. Mak, Spin tunnel field-effect transistors based on two-dimensional van der Waals heterostructures, Nat. Electronics **2**, 159 (2019).

[40] J.-F. Dayen, S. J. Ray, O. Karis, I. J. Vera-Marun, and M. V. Kamalakar, Two-dimensional van der Waals spinterfaces and magnetic-interfaces, Appl. Phys. Rev. **7**, 011303 (2020).

[41] G. Sundaram and Q. Niu, Wave-packet dynamics in slowly perturbed crystals: Gradient corrections and Berry-phase effects, Phys. Rev. B **59**, 14915 (1999).

[42] D. Culcer, J. Sinova, N. A. Sinitsyn, T. Jungwirth, A. H. MacDonald, and Q. Niu, Semiclassical Spin Transport in Spin-Orbit-Coupled Bands, Phys. Rev. Lett. **93**, 046602 (2004).

[43] M.-C. Chang and Q. Niu, Berry curvature, orbital moment, and effective quantum theory of electrons in electromagnetic fields, J. Phys.: Condens. Matter **20**, 193202 (2008).

[44] D. Xiao, M.-C. Chang, and Q. Niu, Berry phase effects on electronic properties, Rev. Mod. Phys. **82**, 1959 (2010).

[45] R. Shindou and K.-I. Imura, Noncommutative geometry and non-Abelian Berry phase in the wave-packet dynamics of Bloch electrons, Nucl. Phys. B **720**, 399 (2005).

[46] Y. Yao, L. Kleinman, A. H. MacDonald, J. Sinova, T. Jungwirth, D.-s. Wang, E. Wang, and Q. Niu, First Principles Calculation of Anomalous Hall Conductivity in Ferromagnetic Bcc Fe, Phys. Rev. Lett. **92**, 037204 (2004).

[47] G. Zhu, S. A. Yang, C. Fang, W. M. Liu, and Y. Yao, Theory of orbital magnetization in disordered systems, Phys. Rev. B **86**, 214415 (2012).

[48] M. Gradhand, D. Fedorov, F. Pientka, P. Zahn, I. Mertig, and B. Györffy, First-principle calculations of the Berry curvature of Bloch states for charge and spin transport of electrons, J. Phys.: Condens. Matter **24**, 213202 (2012).

[49] R. Shindou and L. Balents, Gradient expansion approach to multiple-band Fermi liquids, Phys. Rev. B **77**, 035110 (2008).

[50] F. Freimuth, S. Blügel, and Y. Mokrousov, Spin-orbit torques in Co/Pt(111) and Mn/W(001) magnetic bilayers from first principles, Phys. Rev. B **90**, 174423 (2014).

[51] A. Manchon and S. Zhang, Theory of nonequilibrium intrinsic spin torque in a single nanomagnet, Phys. Rev. B **78**, 212405 (2008).

[52] D. A. Pesin and A. H. MacDonald, Quantum kinetic theory of current-induced torques in Rashba ferromagnets, Phys. Rev. B **86**, 014416 (2012).

[53] K. Shen, G. Vignale, and R. Raimondi, Microscopic Theory of the Inverse Edelstein Effect, Phys. Rev. Lett. **112**, 096601 (2014).

[54] A. Qaiumzadeh, R. A. Duine, and M. Titov, Spin-orbit torques in two-dimensional Rashba ferromagnets, Phys. Rev. B **92**, 014402 (2015).

[55] A. Maleki Sheikhabadi and R. Raimondi, Inverse spin galvanic effect in the presence of impurity spin-orbit scattering: A diagrammatic approach, Condensed Matter **2**, 17 (2017).

[56] T. D. Skinner, K. Olejník, L. Cunningham, H. Kurebayashi, R. Campion, B. Gallagher, T. Jungwirth, and A. J. Ferguson, Complementary spin-Hall and inverse spin-galvanic effect torques in a ferromagnet/semiconductor bilayer, Nat. Commun. **6**, 6730 (2015).

[57] W.-B. Lee, S. B. Kim, K.-W. Kim, K.-J. Lee, H. C. Koo, and G.-M. Choi, Direct observation of spin accumulation and spin-orbit torque driven by Rashba-Edelstein effect in an InAs quantum-well layer, Phys. Rev. B **104**, 184412 (2021).

[58] S. Ghosh and A. Manchon, Spin-orbit torque in a three-dimensional topological insulator–ferromagnet heterostructure: Crossover between bulk and surface transport, Phys. Rev. B **97**, 134402 (2018).

[59] D. Xiao, J. Shi, and Q. Niu, Berry Phase Correction to Electron Density of States in Solids, Phys. Rev. Lett. **95**, 137204 (2005).

[60] K. Y. Bliokh, On the Hamiltonian nature of semiclassical equations of motion in the presence of an electromagnetic field and Berry curvature, Phys. Lett. A **351**, 123 (2006).

[61] C. Duval, Z. Horváth, P. A. Horváthy, L. Martina, and P. C. Stichel, Comment on "Berry Phase Correction to Electron Density of States in Solids," Phys. Rev. Lett. **96**, 099701 (2006).

[62] F. R. Lux, F. Freimuth, S. Blügel, and Y. Mokrousov, Chiral Hall Effect in Noncollinear Magnets from a Cyclic Cohomology Approach, Phys. Rev. Lett. **124**, 096602 (2020).

[63] N. Nagaosa, J. Sinova, S. Onoda, A. H. MacDonald, and N. P. Ong, Anomalous Hall effect, Rev. Mod. Phys. **82**, 1539 (2010).

[64] N. A. Sinitsyn, A. H. MacDonald, T. Jungwirth, V. K. Dugaev, and J. Sinova, Anomalous Hall effect in a two-dimensional Dirac band: The link between the Kubo-Streda formula and the semiclassical Boltzmann equation approach, Phys. Rev. B **75**, 045315 (2007).

[65] N. A. Sinitsyn, Semiclassical theories of the anomalous Hall effect, J. Phys.: Condens. Matter **20**, 023201 (2007).

[66] I. A. Ado, I. A. Dmitriev, P. M. Ostrovsky, and M. Titov, Anomalous Hall Effect in a 2D Rashba Ferromagnet, Phys. Rev. Lett. **117**, 046601 (2016).

[67] M. M. Glazov and L. E. Golub, Valley Hall effect caused by the phonon and photon drag, Phys. Rev. B **102**, 155302 (2020).

[68] E. G. Mishchenko, A. V. Shytov, and B. I. Halperin, Spin Current and Polarization in Impure Two-Dimensional Electron Systems with Spin-Orbit Coupling, Phys. Rev. Lett. **93**, 226602 (2004).

[69] C. Gorini, P. Schwab, R. Raimondi, and A. L. Shelankov, Non-Abelian gauge fields in the gradient expansion: Generalized Boltzmann and Eilenberger equations, Phys. Rev. B **82**, 195316 (2010).

[70] J. Rammer and H. Smith, Quantum field-theoretical methods in transport theory of metals, Rev. Mod. Phys. **58**, 323 (1986).

[71] M. Dyakonov, *Spin Physics in Semiconductors* (Springer-Verlag, Berlin, Heidelberg, 2008).

[72] K. Denisov, I. Rozhansky, N. Averkiev, and E. Lahderanta, Chiral spin ordering of electron gas in solids with broken time reversal symmetry, Sci. Rep. **9**, 10817 (2019).

[73] N. A. Sinitsyn, Q. Niu, J. Sinova, and K. Nomura, Disorder effects in the anomalous Hall effect induced by Berry curvature, Phys. Rev. B **72**, 045346 (2005).

[74] Y. Aharonov and A. Stern, Origin of the Geometric Forces Accompanying Berry's Geometric Potentials, Phys. Rev. Lett. **69**, 3593 (1992).

[75] J. Sinova, D. Culcer, Q. Niu, N. A. Sinitsyn, T. Jungwirth, and A. H. MacDonald, Universal Intrinsic Spin Hall Effect, Phys. Rev. Lett. **92**, 126603 (2004).

[76] D. Culcer and Q. Niu, Geometrical phase effects on the Wigner distribution of Bloch electrons, Phys. Rev. B **74**, 035209 (2006).

[77] K. Kavokin, Spin relaxation of localized electrons in n-type semiconductors, Semicond. Sci. Technol. **23**, 114009 (2008).

[78] K. S. Denisov and N. S. Averkiev, Hall effect driven by non-collinear magnetic polarons in diluted magnetic semiconductors, Appl. Phys. Lett. **112**, 162409 (2018).

[79] L. K. Shi, S. C. Zhang, and K. Chang, Anomalous electron trajectory in topological insulators, Phys. Rev. B **87**, 161115(R) (2013).

[80] G. Vignale and I. V. Tokatly, Theory of the nonlinear Rashba-Edelstein effect: The clean electron gas limit, Phys. Rev. B **93**, 035310 (2016).

[81] G. J. Ferreira, R. P. Maciel, P. H. Penteado, and J. C. Egues, Zitterbewegung and bulk-edge Landau-Zener tunneling in topological insulators, Phys. Rev. B **98**, 165120 (2018).

[82] E. G. Mishchenko and O. A. Starykh, Equilibrium currents in chiral systems with nonzero Chern number, Phys. Rev. B **90**, 035114 (2014).

[83] R. Karplus and J. Luttinger, Hall effect in ferromagnetics, Phys. Rev. **95**, 1154 (1954).

[84] T. Jungwirth, Q. Niu, and A. H. MacDonald, Anomalous Hall Effect in Ferromagnetic Semiconductors, Phys. Rev. Lett. **88**, 207208 (2002).

[85] Q. Niu, D. J. Thouless, and Y.-S. Wu, Quantized Hall conductance as a topological invariant, Phys. Rev. B **31**, 3372 (1985).

[86] M. Offidani and A. Ferreira, Anomalous Hall Effect in 2D Dirac Materials, Phys. Rev. Lett. **121**, 126802 (2018).

[87] J.-i. Inoue, G. E. W. Bauer, and L. W. Molenkamp, Diffuse transport and spin accumulation in a Rashba two-dimensional electron gas, Phys. Rev. B **67**, 033104 (2003).

[88] J. I. Inoue, G. E. W. Bauer, and L. W. Molenkamp, Suppression of the persistent spin Hall current by defect scattering, Phys. Rev. B **70**, 041303(R) (2004).

[89] D. Culcer and R. Winkler, Generation of Spin Currents and Spin Densities in Systems with Reduced Symmetry, Phys. Rev. Lett. **99**, 226601 (2007).

[90] A. Khaetskii, Nonexistence of Intrinsic Spin Currents, Phys. Rev. Lett. **96**, 056602 (2006).

[91] T.-W. Chen, J.-H. Li, and C.-D. Hu, Spin-torque current induced by topological Berry phase in a two-dimensional system with generic k-linear spin-orbit interaction, Phys. Rev. B **90**, 195202 (2014).

[92] X. Wang and A. Manchon, Diffusive Spin Dynamics in Ferromagnetic Thin Films with a Rashba Interaction, Phys. Rev. Lett. **108**, 117201 (2012).

[93] M. Milletarì, M. Offidani, A. Ferreira, and R. Raimondi, Covariant Conservation Laws and the Spin Hall Effect in Dirac-Rashba Systems, Phys. Rev. Lett. **119**, 246801 (2017).

[94] K. Nomura, J. Sinova, T. Jungwirth, Q. Niu, and A. H. MacDonald, Erratum: Nonvanishing spin Hall currents in disordered spin-orbit coupling systems [Phys. Rev. B 71, 041304(R) (2005)], Phys. Rev. B **73**, 199901(E) (2006).

[95] R. Raimondi and P. Schwab, Spin-Hall effect in a disordered two-dimensional electron system, Phys. Rev. B **71**, 033311 (2005).

[96] K. S. Denisov, I. V. Rozhansky, N. S. Averkiev, and E. Lähderanta, General theory of the topological Hall effect in systems with chiral spin textures, Phys. Rev. B **98**, 195439 (2018).

[97] H. Ishizuka and N. Nagaosa, Spin chirality induced skew scattering and anomalous Hall effect in chiral magnets, Sci. Adv. **4**, eaap9962 (2018).

[98] Y. Taguchi, T. Sasaki, S. Awaji, Y. Iwasa, T. Tayama, T. Sakakibara, S. Iguchi, T. Ito, and Y. Tokura, Magnetic Field Induced Sign Reversal of the Anomalous Hall Effect in a Pyrochlore Ferromagnet $Nd_2Mo_2O_7$: Evidence for a spin chirality mechanism, Phys. Rev. Lett. **90**, 257202 (2003).

[99] T. Y. Lee, J. Chang, M. C. Hickey, H. C. Koo, H.-j. Kim, S. H. Han, and J. S. Moodera, Quantum well thickness dependence of Rashba spin–orbit coupling in the InAs/InGaAs heterostructure, Appl. Phys. Lett. **98**, 202504 (2011).

[100] Y. H. Park, S.-H. Shin, J. D. Song, J. Chang, S. H. Han, H.-J. Choi, and H. C. Koo, Gate voltage control of the Rashba effect in a p-type GaSb quantum well and application in a complementary device, Solid-State Electron. **82**, 34 (2013).

[101] Y. Sato, T. Kita, S. Gozu, and S. Yamada, Large spontaneous spin splitting in gate-controlled two-dimensional electron gases at normal in 0.75 Ga 0.25 As/In 0.75 Al 0.25 as heterojunctions, J. Appl. Phys. **89**, 8017 (2001).

[102] W.-Q. Xie, Z.-W. Lu, C.-C. He, X.-B. Yang, and Y.-J. Zhao, Theoretical study of tunable magnetism of two-dimensional MnSe2 through strain, charge, and defect, J. Phys.: Condens. Matter **33**, 215803 (2021).

[103] P. Jiang, L. Li, Z. Liao, Y. Zhao, and Z. Zhong, Spin direction-controlled electronic band structure in two-dimensional ferromagnetic CRi3, Nano Lett. **18**, 3844 (2018).

[104] R. Wiesendanger, Spin mapping at the nanoscale and atomic scale, Rev. Mod. Phys. **81**, 1495 (2009).

[105] S. Girvin and R. Prange, *The Quantum Hall Effect* (Springer-Verlag, New York, 1987).

[106] K. Yang, W. Hu, H. Wu, M.-H. Whangbo, P. G. Radaelli, and A. Stroppa, Magneto-optical Kerr switching properties of (CrI3)2 and (CrBr3/CrI3) bilayers, ACS Appl. Electron. Mater. **2**, 1373 (2020).

[107] N. Mainkar, D. A. Browne, and J. Callaway, First-principles LCGO calculation of the magneto-optical properties of nickel and iron, Phys. Rev. B **53**, 3692 (1996).

[108] G. Y. Guo and H. Ebert, Band-theoretical investigation of the magneto-optical Kerr effect in Fe and Co multilayers, Phys. Rev. B **51**, 12633 (1995).

[109] S. Uba, L. Uba, A. N. Yaresko, A. Y. Perlov, V. N. Antonov, and R. Gontarz, Optical and magneto-optical properties of Co/Pt multilayers, Phys. Rev. B **53**, 6526 (1996).

[110] E. I. Rashba, Properties of semiconductors with an extremum loop. I. Cyclotron and combinational resonance in a magnetic field perpendicular to the plane of the loop, Sov. Phys. Solid State **2**, 1109 (1960).

[111] M. Duckheim and D. Loss, Electric-dipole-induced spin resonance in disordered semiconductors, Nat. Phys. **2**, 195 (2006).

[112] Y. Kato, R. C. Myers, A. C. Gossard, and D. D. Awschalom, Coherent spin manipulation without magnetic fields in strained semiconductors, Nature (London) **427**, 50 (2004).

[113] M. Duckheim and D. Loss, Resonant spin polarization and spin current in a two-dimensional electron gas, Phys. Rev. B **75**, 201305(R) (2007).

[114] M. Schulte, J. G. S. Lok, G. Denninger, and W. Dietsche, Electron Spin Resonance on a Two-Dimensional Electron Gas in a Single Alas Quantum Well, Phys. Rev. Lett. **94**, 137601 (2005).

[115] G. Catarina, N. M. Peres, and J. Fernández-Rossier, Magneto-optical Kerr effect in spin split two-dimensional massive Dirac materials, 2D Mater. **7**, 025011 (2020).

[116] M. Shah and M. S. Anwar, Magneto-optic modulation of lateral and angular shifts in spin-orbit coupled members of the graphene family, OSA Continuum **3**, 878 (2020).

[117] F. R. Pratama, M. S. Ukhtary, and R. Saito, Circular dichroism and Faraday and Kerr rotation in 2D materials with intrinsic Hall conductivities, Phys. Rev. B **101**, 045426 (2020).

[118] L. Falkovsky and A. Varlamov, Space-time dispersion of graphene conductivity, Eur. Phys. J. B **56**, 281 (2007).